geomatics

MDPI

Article

Spatiotemporal Evolution of Post-Mining Deformations in Pécs, Hungary: A Multi-Sensor Approach Using Comparative Assessment of PS-InSAR and Geodetic Data

Dániel Márton Kovács [1,*], István Péter Kovács [2] and Levente Ronczyk [2]

[1] Department of Cartography and Geoinformatics, University of Pécs, 7624 Pécs, Hungary
[2] DATelite Ltd., 7621 Pécs, Hungary
* Correspondence: kdanielm@gamma.ttk.pte.hu

Abstract

Post-mining surface uplift has affected the northeastern part of Pécs, Hungary, since the closure of underground coal mines in the 1990s. This study synthesises 30 years of SAR data (ERS, Envisat, and Sentinel-1) with geodetic surveys, groundwater monitoring, and over 900 residential damage reports to investigate the spatiotemporal evolution of this deformation. In densely built urban environments, Persistent Scatterer Interferometry (PS-InSAR) provides spatially detailed complementary data measurements to traditional levelling, particularly where survey lines offer limited coverage. The performed combined analysis tracked deformation from initial uplift through stabilisation, revealing a clear transition: while early lower-order measurements showed limited correlation, modern Sentinel-1 data and high-order geodetic surveys (post-2014) demonstrate a robust correlation (R = 0.65). The cross-correlation of InSAR results with geodetic and hydrogeological records revealed that aquifer recovery by the 2010s coincided with the onset of surface stability. While over 90% of 1990s residential damage claims fell within measured deformation zones, this relationship weakened over time, with recent claims showing little spatial connection with ground movements. This highlights the complementary strengths of InSAR and geodetic techniques. It demonstrates the value of integrating geotechnical and socio-economic datasets, providing a transferable framework for reliable deformation monitoring and risk management in post-mining urban environments.

Keywords: coal mining; post-mining; surface deformations; uplift; levelling; radar interferometry; PS-InSAR

Check for updates

Academic Editor: João Catalão Fernandes

Received: 23 February 2026
Revised: 16 March 2026
Accepted: 24 March 2026
Published: 27 March 2026

Copyright: © 2026 by the authors. Licensee MDPI, Basel, Switzerland. This article is an open access article distributed under the terms and conditions of the Creative Commons Attribution (CC BY) license.

1. Introduction

Post-mining surface deformations—manifesting as either subsidence or uplift—pose complex geotechnical challenges that require integrated monitoring strategies to safeguard infrastructure in former mining areas [1,2]. The resulting ground strain and differential movements can compromise critical assets and lead to substantial repair costs for buildings and utilities [3,4]. Surface deformations related to mining activities have been documented using traditional geodetic techniques such as precise levelling [5,6] and GNSS (Global Navigation Satellite System) [7–9], which remain highly reliable for long-term monitoring at discrete locations, particularly with recent advances in low-cost GNSS systems [10]. However, while highly accurate, these methods are labour-intensive and require regular maintenance to ensure data quality [11,12]. While recent advancements in networked

automatic deformation monitoring systems (NADMS) have significantly improved the efficiency of ground-based sensors [11], these systems remain spatially constrained to discrete locations and, by design, operate only prospectively.

As an alternative, spaceborne SAR applications—particularly PS-InSAR [13]—have become widely used, offering millimetre-scale precision over large areas and serving as an effective complement or alternative for conventional techniques [14–17]. Consequently, in geosciences, PS-InSAR has become a state-of-the-art technique for monitoring diverse natural processes [18–20], tracking anthropogenic surface deformations of various scales and origins [21–25], and, more specifically, for detecting ground movements associated with coal mining [26–29]. Despite its extensive spatial coverage, integrating InSAR results with legacy geodetic datasets remains challenging, especially in complex urban environments where near-surface processes, such as swelling clays, complicate the interpretation [30,31].

Consequently, research gaps persist in developing long-term multi-source frameworks required to capture the full life-cycle of post-mining stabilisation [2] and a cohesive coupling of the deformation–hydrology–social impacts; as such, geomechanical measurements and hydrogeological datasets are rarely connected with subsequent socio-economic consequences, such as damage to residential properties [11,32,33].

This study addresses these shortcomings by situating diverse datasets within a unified evaluative framework to analyse a geologically complex urban area affected by decades of surface uplift resulting from the artesian hydrostatic rebound of the aquifer. Beyond generalised observations, we provide three specific contributions in methodological synthesis and the application of results:

i. Establishing a continuous 30-year evolutionary record by harmonising three generations of spaceborne SAR data (ERS, Envisat, and Sentinel-1) with legacy geodetic levelling into a single consistent framework.
ii. Conducting a spatiotemporal inter-comparison and integration of multi-temporal PS-InSAR and levelling data to reveal the evolution of uplift to its definite stabilisation and to corroborate its hydrogeological drivers.
iii. Analysing the spatial correspondence between deformation patterns and groundwater recovery with a long-term archive of over 900 residential damage reports.

By mapping these overlapping datasets, this research demonstrates a comprehensive approach, serving as an objective tool for mining-related deformation evaluation and providing a robust scientific basis for urban planning in post-mining environments.

Site Description

The study area, located in southern Hungary on the southern slopes of the Mecsek Mountains in the northeastern part of Pécs, covers 14 km^2 and includes primary mining zones, associated infrastructure, and surrounding residential neighbourhoods (Figure 1). Nearly two centuries of coal mining shaped the region's geomorphology, caused surface deformations and damaged hundreds of buildings [34–36]. Industrial extraction evolved from mid-19th century open-cast operations to modern deep-shaft mining, which required continuous dewatering [37,38]. Underground mining induced delayed subsidence, contingent upon the specific rheological properties of the overburden [39]. Although coal production peaked in the 1960s, a steady decline followed due to reduced geological viability and national economic restructuring. Operational periods and closures varied among mining shafts, but the last underground operation in the study area ceased by 1993 [40]. Consequently, no deep-shaft mines were operational during this study's timeframe; only one open-pit extraction continued throughout the 1990s until its closure in 2004. The cessation of mine-water pumping in 1992 initiated hydrostatic rebound in the Mecsek Coal

Formation Aquifer (MCFA), triggering the progressive surface uplift observed throughout the 1990s and 2000s [40,41].

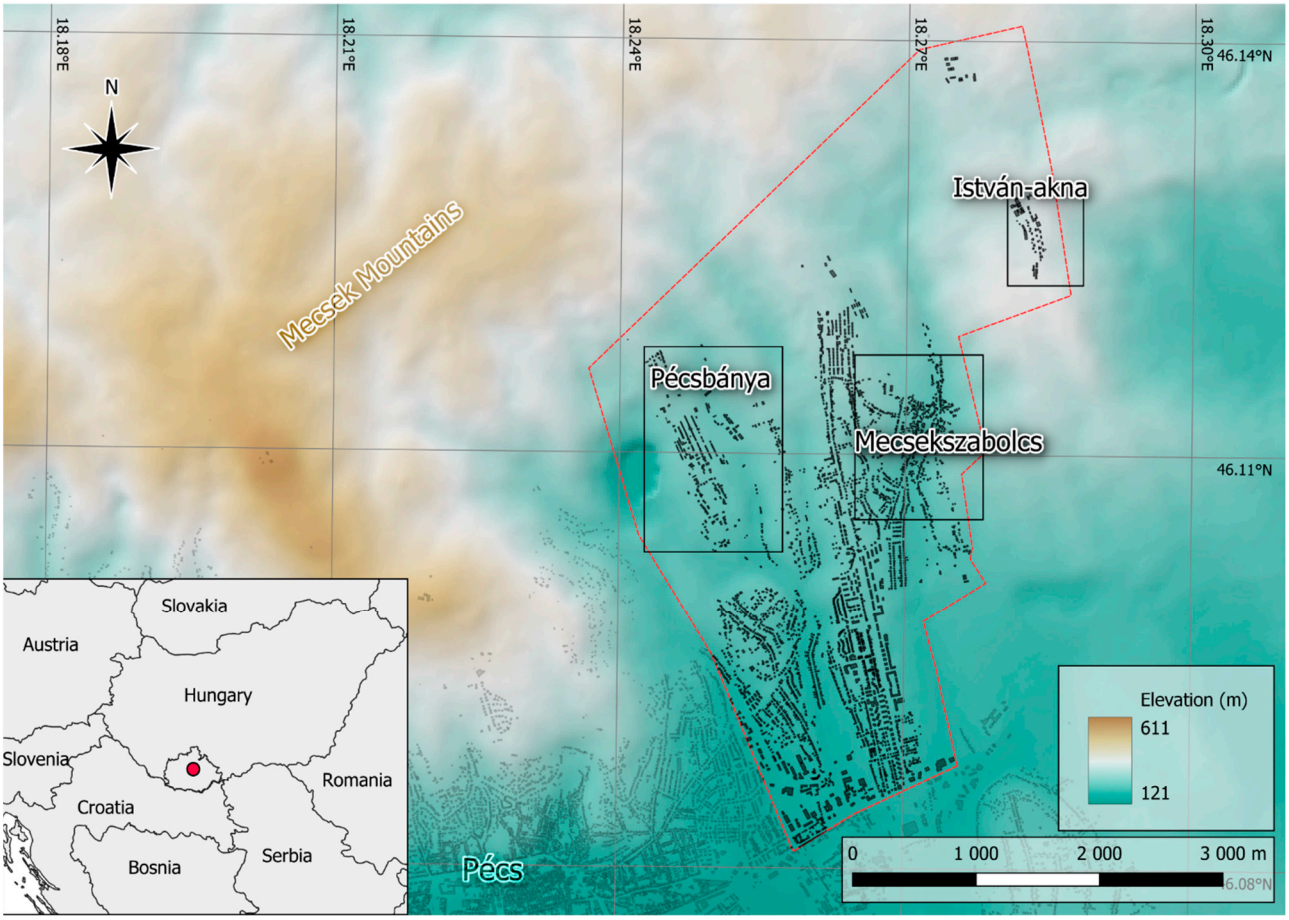


Figure 1. The location of the study area (marked by the red dashed line) is in the northeast part of the city of Pécs. Three high-interest sub-districts are marked and labelled to clarify their location for this article.

Geologically, the study area represents Hungary's only bituminous coalfield, situated within the compressional Mecsekszabolcs Basin. The Early Jurassic Mecsek Coal Formation (MCF) exceeds 1000 m in thickness, containing several hundred coal seams (ranging from 0.05 to 7 m), interbedded with barren strata [40]. Neogene compression induced significant faulting and folding, characterised by north–south faults and east–west thrusts, resulting in steeply dipping coal seams (average: 47°) [38].

The MCF is underlain by the impermeable Late Triassic Karolinavölgyi Sandstone Formation and overlain with a sequence of permeable Neogene and impermeable Middle Miocene (Badenian) sediments; the latter acts as a caprock for the MCFA (Figures 2 and 3). Late Miocene marine and younger deposits reach thickness of 250 m in the south, whereas erosion in the north has exposed the MCF and the Badenian layers. Most of the surface is covered by Quaternary terrestrial deposits, anthropogenic landfills, and swelling clay layers (~2.5 m thick), capable of causing vertical surface movements of ±15–25 mm [39]. Critically, local groundwater is hydraulically isolated from MCFA fluctuations by the impermeable Badenian layers, responding instead primarily to precipitation, evapotranspiration, and local hydrogeological conditions [38,39].

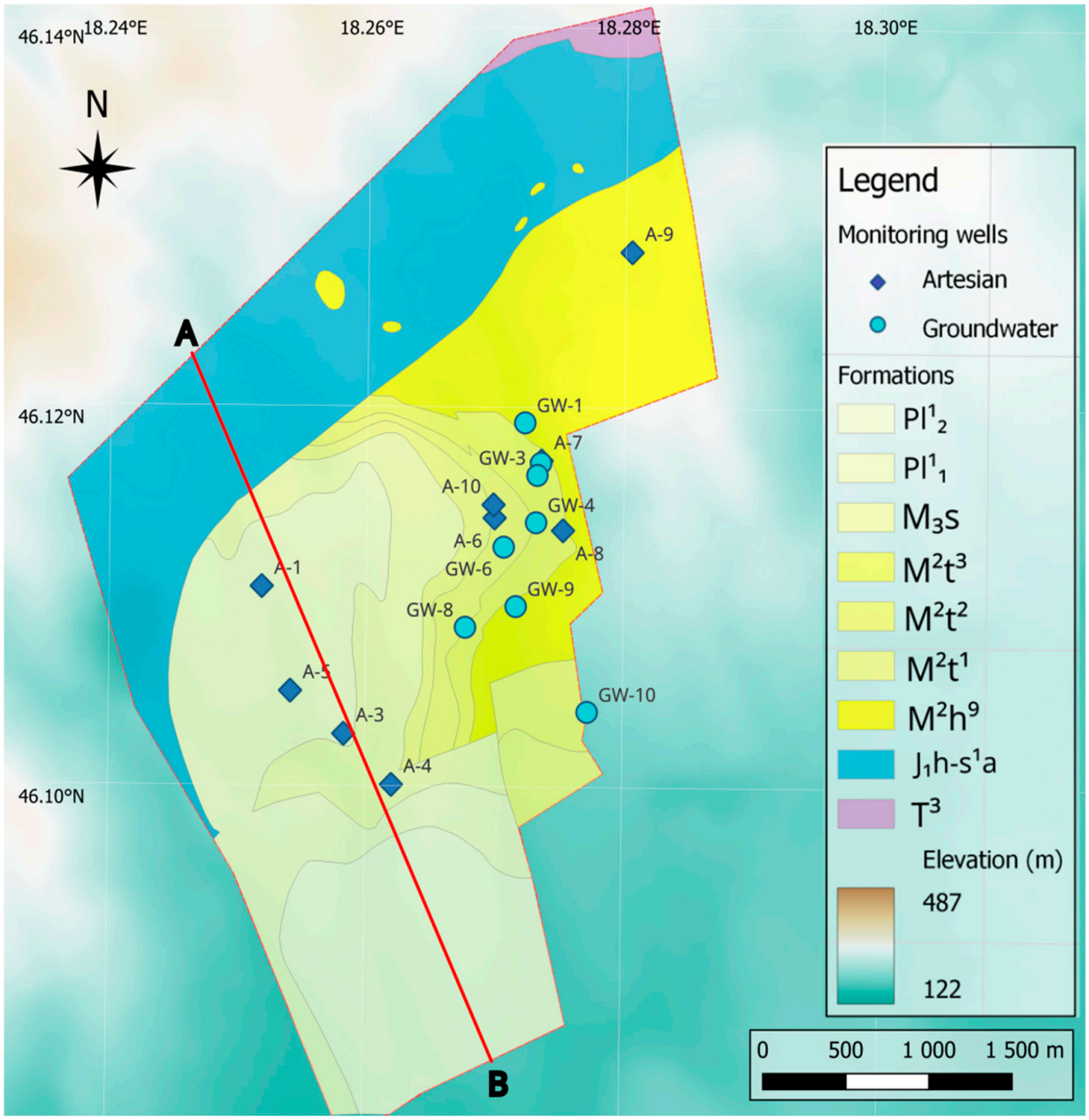


Figure 2. A 1:10,000 scale geological map of the research site edited based on [42] showing the location of the artesian and groundwater monitoring wells. The red line marks the cross-section shown in Figure 3, where the specific geological formations are also described.

The continuous dewatering of the MCFA began in the mid-19th century. The deepest mine shafts reached a depth of around 500 m, depressing the piezometric surface to approximately 200 m below sea level [38]. Water abstraction peaked in the 1960s at an average rate of ~4 m^3/min, followed by a reduced operational rate of ~2–2.5 m^3/min until pumping ceased entirely in 1992 [39]. The cessation of pumping triggered an immediate hydrostatic rebound, with rapid recovery during the 1990s and near-stabilisation by the mid-2000s. The post-mining uplift phase was triggered by increased pore pressure within the disturbed coal-bearing strata during the groundwater rebound. In the Pécs–Mecsekszabolcs area, this process resulted in significant surface deformations from 1993 onwards [38].

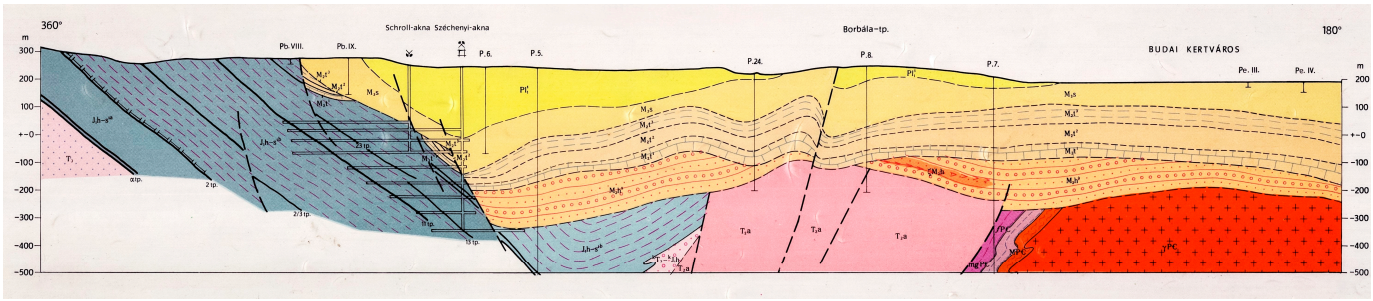


Figure 3. Geological cross-section along the A–B line (for location, see Figure 2) [42]. Description of original annotations: *Schroll-akna* and *Széchenyi-akna* denote historical mine shafts; *Borbála-tp.* (Borbála-telep) refers to a former mining settlement; *Budai Kertváros* indicates a densely developed residential area. $Pl^1{}_2$—Upper Pannonian limonite sand; $Pl^1{}_1$—Lower Pannonian sandstone, aleurite, and clay marl; M_3s—Sarmatian porous oolitic limestone; M_2t^3—Middle Miocene limestone clay marl; M_2t^2—Middle Miocene fine sand with lingerie interbeddings; M_2t^1—Middle Miocene calcareous sandstone; M_2h^9—Early Miocene gravel, conglomerate, sand, and sandstone; ζM_2h—Early Miocene dacite tuff and tuffite; M_2h^6—Early Miocene scaly clay marl; M_2h^1—Early Miocene gravel, conglomerate, sandstone, and aleurite; J_1s^{2f}—Jurassic calcareous marl; $J_1s^{2d–e}$—Jurassic marl with calcareous marl pans; J_1s^{2c}—Jurassic clay marl; $J_1h\text{-}s^{1b}$—Jurassic coal seam (middle member); $J_1h\text{-}s^{1a}$—Jurassic coal seam (lower member); ${}^kT_3$ ${}^kJ_1h$—Triassic conglomerate with limestone gravels and calcareous sandstone; T_3—Triassic sandstone, aleurite, and schistose clay; T_2a—Triassic dolomite and limestone; ${}^{\int}P\varepsilon$—Precambrian phyllite and amphibolite; $MP\varepsilon$—Precambrian Migmatite; ${}_{\gamma}P\varepsilon$—Precambrian granodiorite, syenite, and granite; ${}_{mg}P\varepsilon$—Precambrian schist and gneiss.

2. Materials and Methods

2.1. Geodetic Survey Data

A geodetic levelling network was established in northeastern Pécs during the operational phase of mining to monitor subsidence and delineate the affected zones [36]. Following the closure, the network (Figure 4) remained critical for tracking post-mining surface deformations [39]. The network was redesigned in 2008; since then, high-order levelling has been conducted biannually along three revised lines. The enhanced precision is capable of detecting submillimetre-scale vertical displacements and a maintained accuracy of ±2 mm/km—equating to ±2–6 mm for line lengths of 1–3 km [39].

The dataset, spanning over three decades, was provided by BVH (the legal successor of the former state-owned mining company) and serves as a key reference for assessing long-term surface movements. All measurement lines used in this study were already operational at the start of the ERS observation period; however, due to the lack of precise dates, especially in early annual surveys in the 1990s, the measurement dates closest to the SAR acquisitions were selected to ensure the highest possible temporal consistency.

A total of 132 geodetic points with consistent data coverage were processed from measurements conducted prior to 2008, while 116 points were available from the updated geodetic network after 2008. To evaluate potential correlations between the surface deformations detected by geodetic surveys and the spatial distribution of public complaints, displacement zones were delineated based on interpolated average velocity values for each geodetic point during the ERS (1992–2001) and Envisat (2002–2010) observation periods. Subsequently, complaints were classified according to these displacement zones and analysed to assess the relationship between reported damage cases and observed surface displacements.

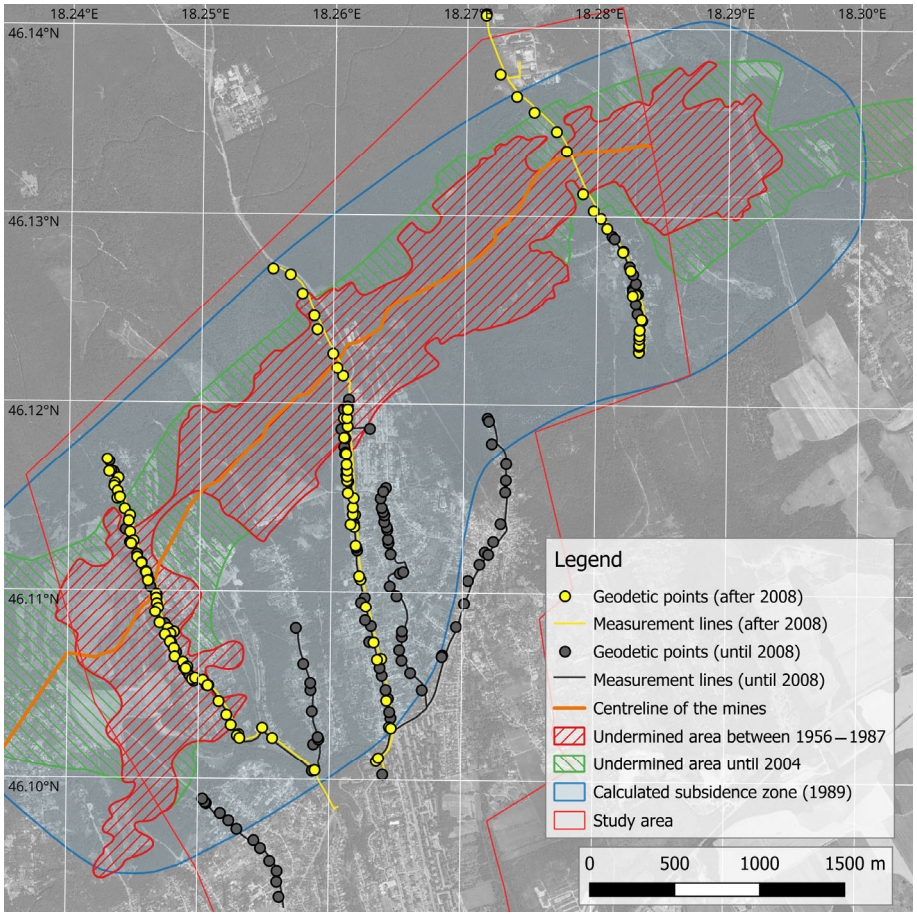


Figure 4. The network of measurement lines and points across the study area in respect to the extent of mining activity.

2.2. Satellite Data

To analyse ground movements, Synthetic Aperture Radar (SAR) imagery acquired over the past 30 years from the ERS, Envisat, and Sentinel-1 missions were utilised to investigate surface deformation within the study area. ERS and Envisat data were sourced from the European Space Agency's (ESA) Online Dissemination Portal [43], while Sentinel-1 Single Look Complex (SLC) images were obtained from the Alaska Satellite Facility's (ASF) Vertex server [44] (Table 1).

Table 1. Overview of downloaded images.

Sensor	Geometry	Relative Orbit	Start Date	End Date	Number of Scenes
ERS	Ascending	229	31 May 1995	18 July 2001	21
ERS	Descending	451	24 November 1992	1 December 2000	52
Envisat	Ascending	458	6 December 2002	8 January 2010	21
Envisat	Descending	451	1 November 2002	23 April 2010	36
Sentinel-1	Ascending	73	10 October 2014	1 January 2022	364
Sentinel-1	Descending	51	9 October 2014	12 January 2022	354

2.2.1. Processing Techniques

Interferometric stacking algorithms, such as the Persistent Scatterers (PS) or SBAS (Small Baseline Subsets) [45], are specifically designed to detect and quantify small-scale

surface displacements with high precision. By leveraging multiple SAR images, these algorithms overcome the limitations of conventional differential InSAR (DInSAR) methods, primarily by modelling and mitigating atmospheric phase noise. PS algorithms target scatterers exhibiting stable geometry and high phase coherence, which are abundant in urban environments [16]. Consequently, this approach is considered as the industry standard for high-precision monitoring and is extensively utilised for detecting displacements in urban environments [22,46–48]. Consequently, in our research, PS-InSAR was prioritised over SBAS or D-InSAR techniques, due to the urban characteristics of the study area. Furthermore, while advanced second-generation MT-InSAR algorithms—such as SqueeSAR™ [49]—offer enhanced measurement density in rural or sparsely vegetated areas, they often require proprietary software or entail significantly higher computational capacity [50,51]. In the densely built environment of Pécs, the standard PS-InSAR approach yielded a sufficiently high density of scatterers to characterise the displacements; therefore, the implementation of more complex DS algorithms was deemed unnecessary, as they would not have significantly altered the conclusions of this study.

2.2.2. Interferometric Processing

PS-InSAR processing was performed for each sensor and geometry using SARScape® 5.7 (with ENVI 5.7.0), with topographic phase removal and geocoding based on the SRTM-3 (v4) DEM [52]. The final outputs included 2D vector point clouds of displacement time series and quality metrics for each scatterer.

Concerning the methodological choice, it is important to note that the ERS and Envisat ascending datasets contained fewer than 25 acquisitions, a number close to the practical lower limit for reliable PS processing. As a preliminary step, and for a more thorough approach, SBAS was applied to these datasets to evaluate its suitability. While SBAS provided slightly broader spatial coverage in peripheral areas, it did not provide a substantial improvement in measurement accuracy. In the densely built-up core of the study area—the primary focus, which coincides with the main levelling network and the majority of residential damage claims—the PS technique yielded more precise velocity estimates and displacement measurements than SBAS. This represents an important advantage, particularly when modelling longer time spans from a limited number of acquisitions, as even small annual velocity differences can lead to significant long-term discrepancies and complicate direct comparisons with geodetic measurements. While the spatial coverage of PS was somewhat lower than SBAS, it was more than sufficient to delineate the deformation zones of interest, owing to the high density of persistent scatterers such as building facades and infrastructure within the undermined districts.

While integrating ascending and descending datasets to derive two-dimensional (vertical and east-west) deformation components can improve completeness, such decomposition was not feasible for ERS and Envisat due to inconsistent overlap and sparse acquisition schedules. Attempting a decomposition into vertical and east–west components under such constraints would have yielded unreliable results. Instead, to maximise the spatial coverage while preserving the measurement integrity the ascending and descending datasets from each sensor were merged separately after confirming a high degree of velocity consistency within each pair, substantially increasing the density of deformation observations. The close agreement between the ascending and descending datasets, as outlined in Section 3.1, supports this methodological choice.

2.3. Data Analysis

To enable a detailed spatial analysis of surface deformations, a zone-based evaluation of all PS points was conducted. The centreline of the undermined zones was first delineated

using a medial axes approach, after which buffer zones were generated at 500 m intervals to encompass the entire study area. Within each buffer, PS velocity values were statistically analysed to determine how deformation patterns varied with increasing distance from the centreline. This approach delineated the extent and intensity of post-mining subsidence, clearly identifying the zones most impacted by mining-induced ground deformation.

To evaluate the multi-sensor PS-InSAR results across multiple decades, this study employed a robust cross-validation framework using geodetic levelling as the primary reference. Assuming a correlation between levelling measurements and adjacent PS velocities, a 30 m buffer was established around each geodetic point. Within these buffers, averaged PS velocities were compared with the corresponding annual geodetic point velocities. Mean velocities of grouped PS points within each buffer were calculated to facilitate direct comparison with the levelling data. Statistical analyses, including correlation and determination coefficients, linear regression, and root mean square error were applied to assess the consistency and agreement between the datasets. Ultimately, these evaluations provided a consistent baseline of accuracy, confirming the reliability of the InSAR trends across the varying temporal scales of the study.

Deformation zones were delineated based on interpolated (multilevel b-spline method) annual velocities from ERS and Envisat-era InSAR data alongside the concurrent geodetic measurements, and a uniform velocity threshold of ± 1.5 mm/year was used to define four distinct deformation zones based on the data acquisition era and method. This methodology enabled the visualisation of the measured deformations in relation to the location of damaged properties and the associated claim outcomes. Given the consistently stable surface conditions and the very limited number of damage reports, extending the analysis to the Sentinel-1 era of the 2010s was considered unnecessary.

To integrate the PS-InSAR datasets with the levelling network, a Regression Kriging (RK) approach was also implemented [53] using SAGA GIS (v.9.11.3). RK is a spatial prediction technique that combines regression of the dependent variable on auxiliary variables with kriging of regression residuals. This hybrid geostatistical method was selected based on its proven capability to combine heterogeneous data sources—levelling and PS-InSAR in our case—while rigorously accounting for the varying precision of each sensor [54,55]. During the parametrisation of the process, the Gaussian variogram model was selected to ensure methodological consistency and the possibility of precise cross-comparison across the multi-decadal datasets.

2.4. Groundwater and Artesian Monitoring Wells

Post-mining aquifer regeneration was assessed using data from eight groundwater wells in the eastern study area and ten artesian wells distributed regionally (Figure 5). Historical well data from 2006—provided by BVH—were only sufficient to reconstruct the late stages of hydrostatic rebound and the transition into the 2010s, when all monitored water levels stabilised. Therefore, these records offer no information on the onset of movement or the initial large-scale deformations of the 1990s. Statistical comparisons with surface displacement data were therefore restricted to the stable period, exclusively focusing on analysis with Sentinel-1-based PS velocities. Given the contrasting hydrodynamic behaviour of the two aquifer systems and the absence of significant long-term trends in both artesian well levels and Sentinel-1 PS velocities, any detected surface displacement or InSAR time-series fluctuations after 2014 were primarily attributed to seasonal changes in the groundwater table or some localised fluctuation of the MCFA.

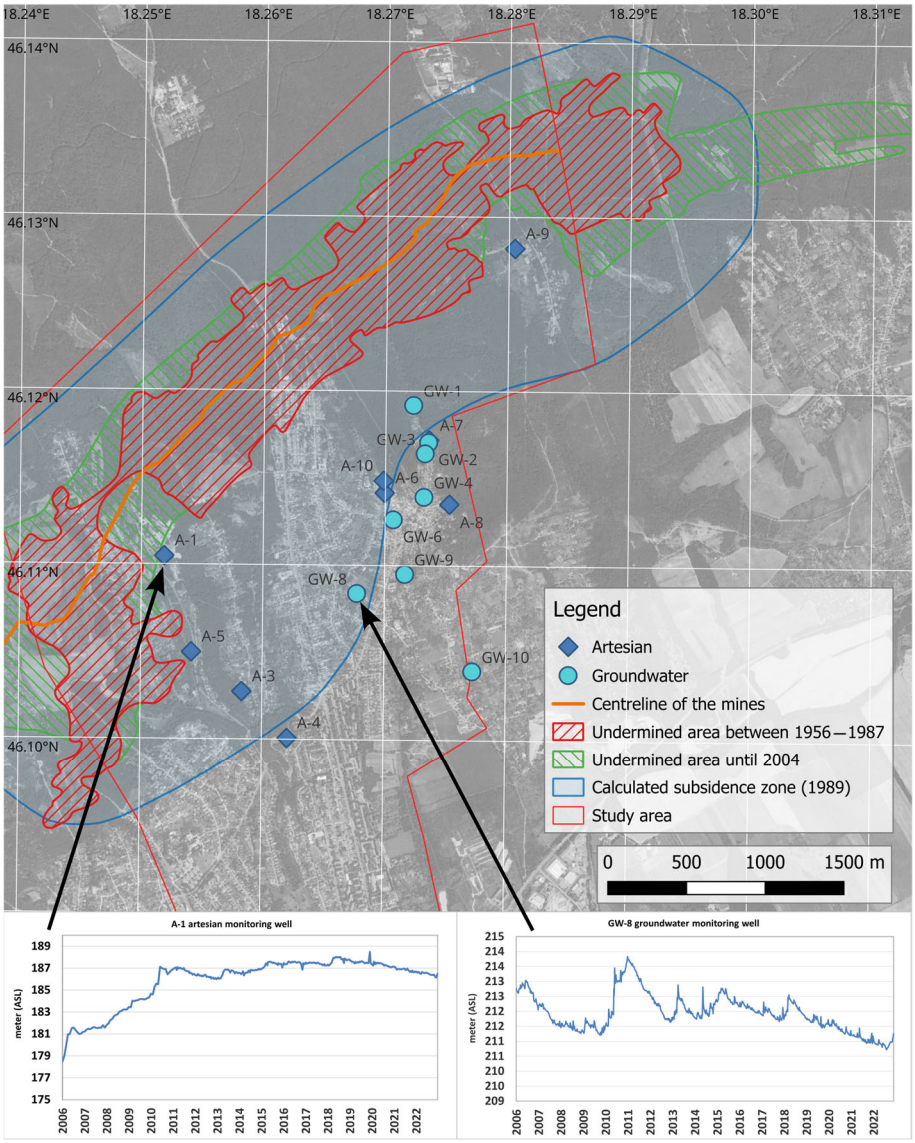


Figure 5. Groundwater and artesian well locations overlaid on undermined zones and the calculated subsidence zone. Time series plots show hydraulic head levels at wells A-1 and GW-8, while the arrows indicate the spatial position of the two wells.

Correlation analysis between water levels and InSAR-derived surface deformations were carried out using buffer zones delineated around each monitoring well. PS points located within 30 m of the wells were selected to ensure spatial consistency between the remote sensing observations and in situ hydrological data. These localised datasets formed the basis of the correlation assessment.

2.5. Complaints Regarding Building Damage

The study area comprises a network of small colonies and villages, which developed primarily due to mining operations or to accommodate the growing population. Since the 1990s, the city's population has steadily declined; so, the overall extent of the built-up area has remained largely unchanged. Only incremental changes and gradual modernisation of buildings have occurred. The building stock is highly heterogeneous and lacks typical urban characteristics, often resembling rural settlements. The diversity of construction materials, techniques and foundation types, often of varying quality, has significantly influenced how individual structures have responded to surface deformations over time [39].

Despite the cessation of underground operations in 1992, residential claims continued to accumulate across the study area in the following decades. For this analysis, 914 cases submitted (data courtesy of BVH) over the past 30 years were processed and selected based on their spatial and temporal alignment with InSAR data. Complaint locations were georeferenced to produce a point layer of their distribution. Cases were categorised by outcome (compensated or denied) and primary cause (water-related or structural) and then overlaid onto the four deformation zones defined in Section 2.3. to assess whether measured ground displacements influenced their occurrence or resolution. The goal was to identify potential correlations between surface deformation and claim outcomes.

3. Results

In this study, we conducted a 30-year analysis of surface deformations in a heavily undermined urban area, synthesising multi-sensor data from ERS, Envisat, and Sentinel-1 to assess the evolution and stabilisation of post-mining deformations. Section 3.2 compares the InSAR and geodetic measurements, while Section 3.3 explores the temporal correlations between monitoring data and water level changes. Section 3.4 evaluates the impact of deformation on hundreds of residential complaints.

3.1. Interferometric Results

PS-InSAR analysis revealed significant spatiotemporal variations in surface deformation, defined primarily by a progressive uplift in the 1990s and a transition to widespread stabilisation by the mid-2010s. During the 1990s, velocity values were characterised by broad ranges, with peak velocities reaching +13.6 mm/year (descending) and +12.9 mm/year (ascending), closest to the undermined area. While the average velocities for the study area appear low, these mean values are mathematically suppressed by a significant amount of relatively stable points on the southern end of the study area (Table 2). Consequently, the extremes of the velocity range more accurately represent the true intensity of the early artesian rebound.

Table 2. Descriptive statistics of the interferometric results by sensor and geometry.

	ERS		**Envisat**		**Sentinel-1**	
Geometry	Asc. (229)	Desc. (451)	Asc. (458)	Desc. (451)	Asc. (73)	Desc. (51)
PS/km^2	66	225	32	260	693	745
Avg.vel. (mm/year)	1.26 mm	0.59 mm	−0.12 mm	0.19 mm	−0.054 mm	0.015 mm
Range (mm/year)	−5.13–12.9	−3.8–13.6	−2.9–4.6	−4.4–4.1	−3.9–2.9	−3.8–3.1

The deceleration of aquifer recovery is directly reflected in the contraction of these velocity ranges. During the Envisat-era (2002–2010), the maximum uplift velocities decreased significantly to +4.6 mm/year, and the data showed that the largest displacements remained in the northern study area but became more concentrated and shifted west–northwest, indicating gradual surface consolidation. This stabilisation trend reached its definitive phase during the Sentinel-1-era (2014–2022), when the maximum velocity values further declined to 3.1 mm/year.

The high degree of velocity consistency observed between the ascending and descending geometries across all three satellite generations justifies the merging of these datasets to maximise the point density and provide a comprehensive 30-year record of the stabilisation process (Figure 6).

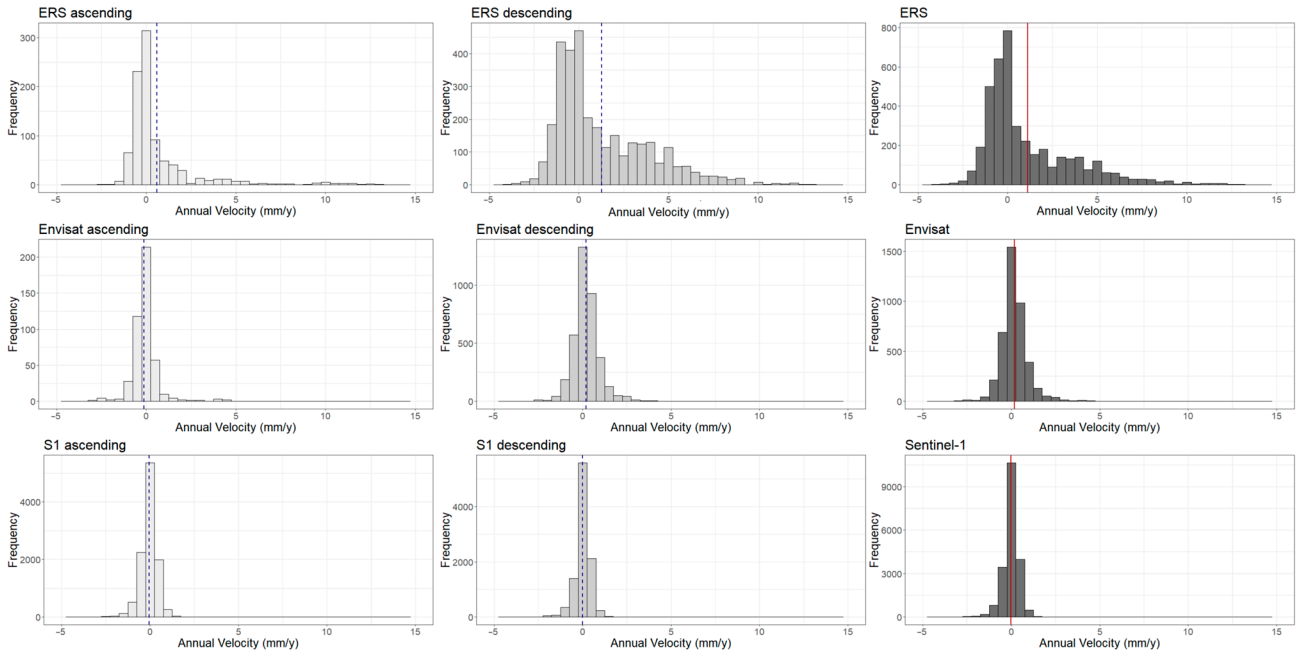


Figure 6. Histogram of the velocity values according to the geometries and after merging. The dashed lines and the red vertical lines mark the average of each dataset.

Interferometric Post-Processing

In the 1990s, ERS data revealed pronounced uplift near the mines, with mean velocity values decreasing with the distance from the undermined area. Within 500 m of the calculated centreline, the mean uplift reached 7.95 mm/year, declining to 5.8 mm/year at 1000 m and 3.65 mm/year at 1500 m. Beyond 1500 m, the velocities stabilised, converging to approximately 1.15 mm/year up to the 3000-m buffer. During the 2000s, Envisat data indicated reduced displacement magnitudes over a smaller area. The mean velocities decreased from 1.58 mm/year within 500 m to 1.28 mm/year at 1000 m, 0.8 mm/year at 1500 m, and 0.16 mm/year beyond 3000 m. Sentinel-1 data showed near-complete stability, with mean velocities around −0.002 mm/year even within the 500 m zone and minimal variation across the study area (Figure 7).

To quantitatively evaluate the spatial attenuation of surface movements, a regression analysis with a third-order polynomial model was performed by correlating the PS displacement velocities with the distance from the mine's centreline. This mathematical relationship provides a quantitative confirmation that the influence of post-mining rebound systematically fades within a 2500 m range, providing a robust theoretical validation for the empirically derived deformation boundaries.

3.2. Comparing InSAR Data with Geodetic Measurements

According to measurement reports, the precision of geodetic levelling was ±2 mm/km [39]. With an average section length of 2.4 km, displacements of 4–6 mm could result in a relative error of up to 100%. Additional uncertainties arose from insufficient stability or potential damage to levelling marks. Interpreting vertical displacements therefore required consideration of the cumulative measurement errors (±4–6 mm), seasonal clay swelling (±15–25 mm), and actual post-mining ground movements. These combined effects could produce apparent displacements of up to ±30 mm, complicating the detection of long-term trends. The 2008 technical report also noted that complex subsoil conditions were not adequately considered in the initial network design [39].

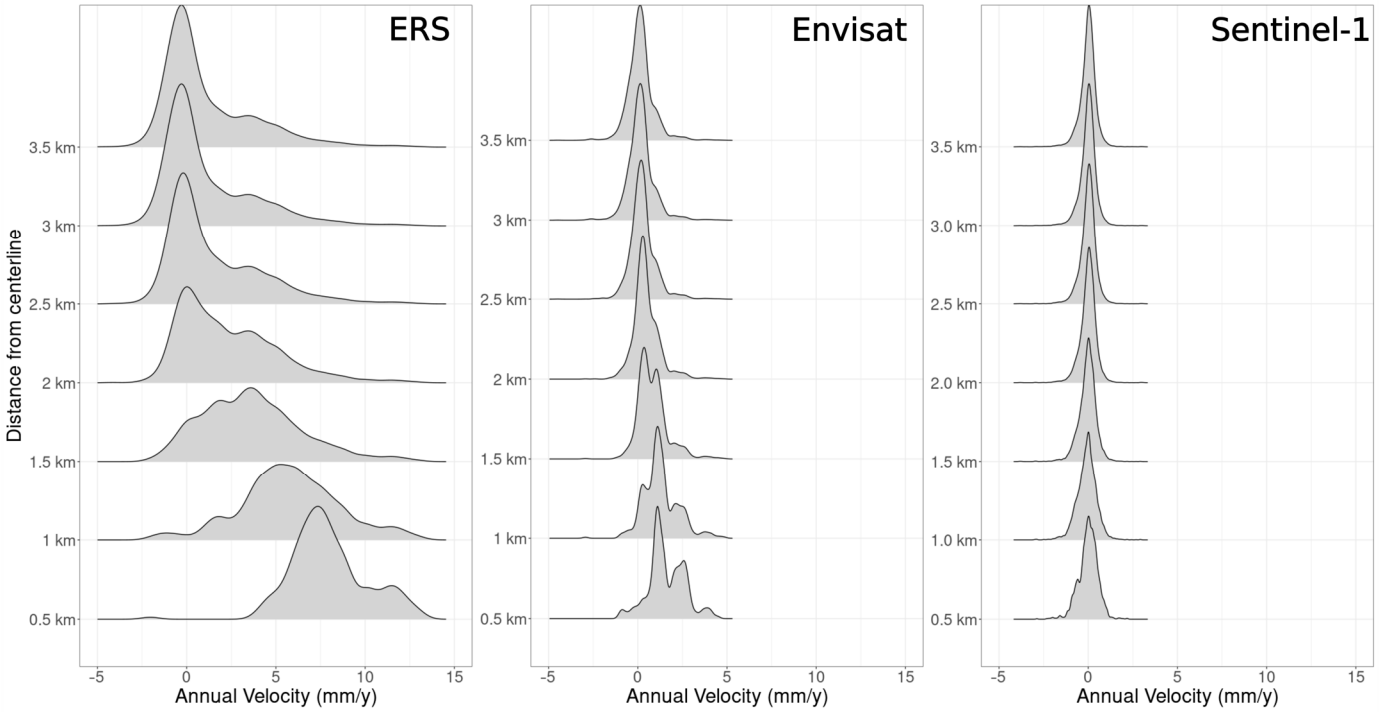


Figure 7. Annual velocity distributions of PS points at 500 m intervals from the mine centreline, shown for ERS, Envisat, and Sentinel-1 datasets.

Comparisons between the geodetic and InSAR datasets (ERS, Envisat, Sentinel-1) revealed notable differences. The geodetic data showed higher standard deviations (σ = 2.12 for 1990s, σ = 1.26 for 2000s, σ = 1.03 after 2014) than InSAR (σ = 2.38, 0.68, and 0.44, respectively). Base points used for geodetic measurements, located just outside the undermined area, remained stable over the 30 years, with average PS velocities of 0.15 mm/year (ERS), −0.29 mm/year − (Envisat), and −0.13 mm/year (Sentinel-1) within a 100 m radius respectively.

For direct comparison, 177 ERS PS points within 30 m of 112 geodetic points were analysed, corresponding to locations with consistent 1990s data (Figure 8).

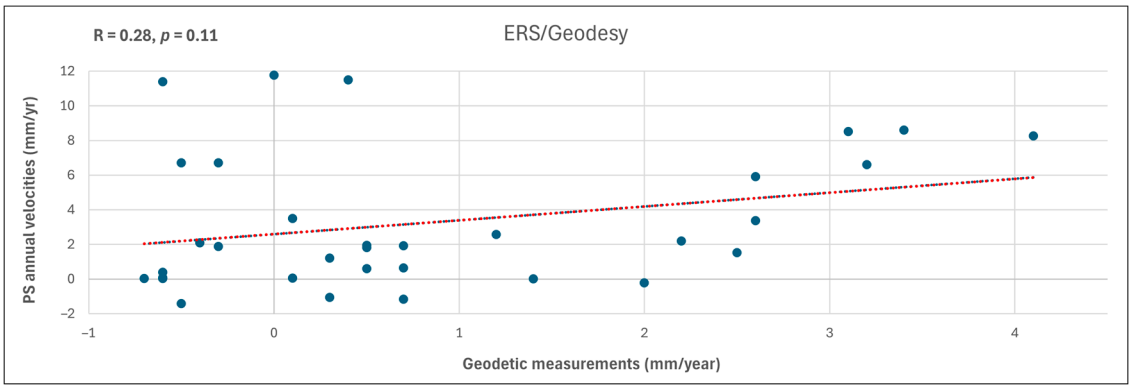


Figure 8. A scatter plot of geodetic points from the ERS period and the PS points averaged within their 30 m buffer zones. The red dashed line indicates the linear trendline.

These comparisons showed differences: the geodetic data indicated only a mild uplift (3–5 mm/year), while the InSAR velocities at the same locations averaged 7–12 mm/year (Figure 9).

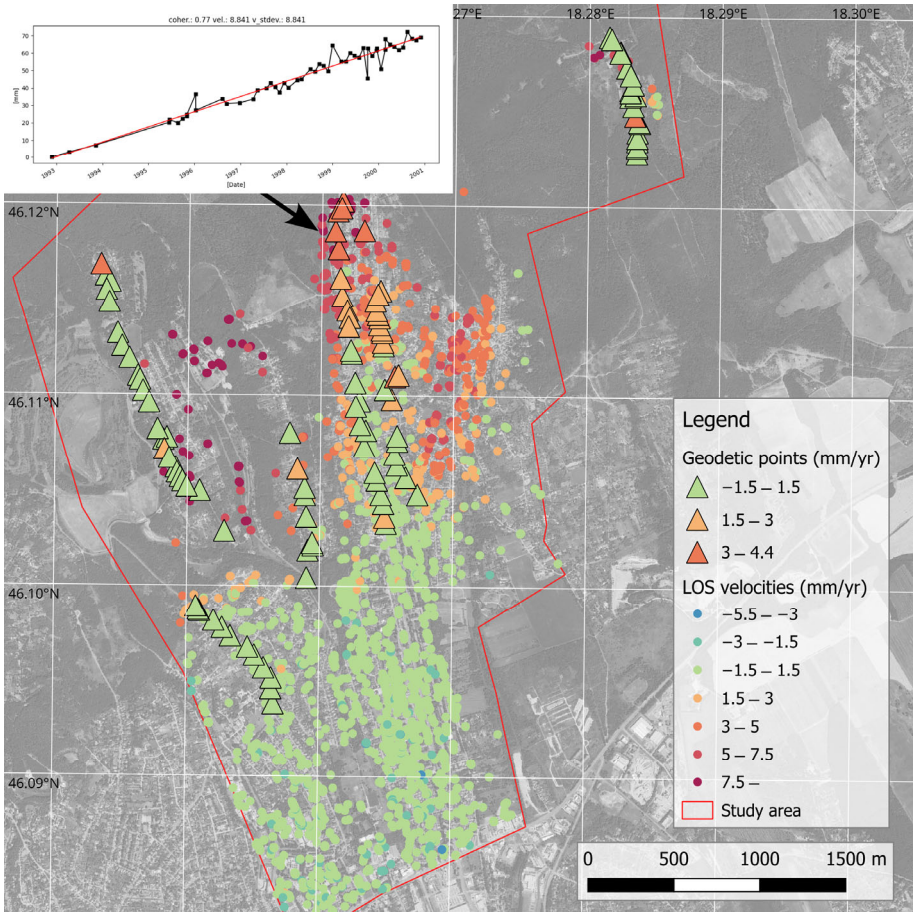


Figure 9. The annual velocity of the PS points and the average annual displacements of the geodetic points from 1992 until 2001, covering the ERS era. The inset graph (top left) displays the displacement time series for a selected PS point indicated by the black arrow, where the red line represents the fitted linear velocity trend.

The correlation coefficient between the two datasets was R = 0.28 ($p > 0.05$), indicating a statistically insignificant weak positive relationship. The absolute RMSE was 4.434 mm against a total geodetic range of 13.19 mm, resulting in a normalised RMSE of 33.62%.

During the Envisat era, 200 PS points were identified within 30 m of 99 geodetic points—a decline from the ERS period due to the lack of continuous measurements at some points. PS velocities exhibited narrower ranges, lower standard deviations, and different averages compared with concurrent geodetic data. From the early 2000s, the deformation patterns gradually shifted northwest, although the limited number of available SAR scenes constrained the PS point density (Figure 10). Geodetic records also indicated declining velocities and increasing stability, albeit with periodic fluctuations similar to those observed during the 1990s.

During the Envisat era (2002–2010), the statistical agreement remained limited, yielding a correlation coefficient of R = −0.14 ($p > 0.05$), indicating a lack of a linear relationship between the two datasets (Figure 11). The RMSE was 1.904 mm, effectively matching the narrow velocity range (1.96 mm) of the levelling points as the surface began to consolidate. Consequently, the normalised RMSE reached 97.15%; a sharp increase compared to the ERS era. These metrics suggest that during this period, the measured discrepancies were dominated by instrumental noise and the precision limits of the legacy geodetic network rather than active surface deformation.

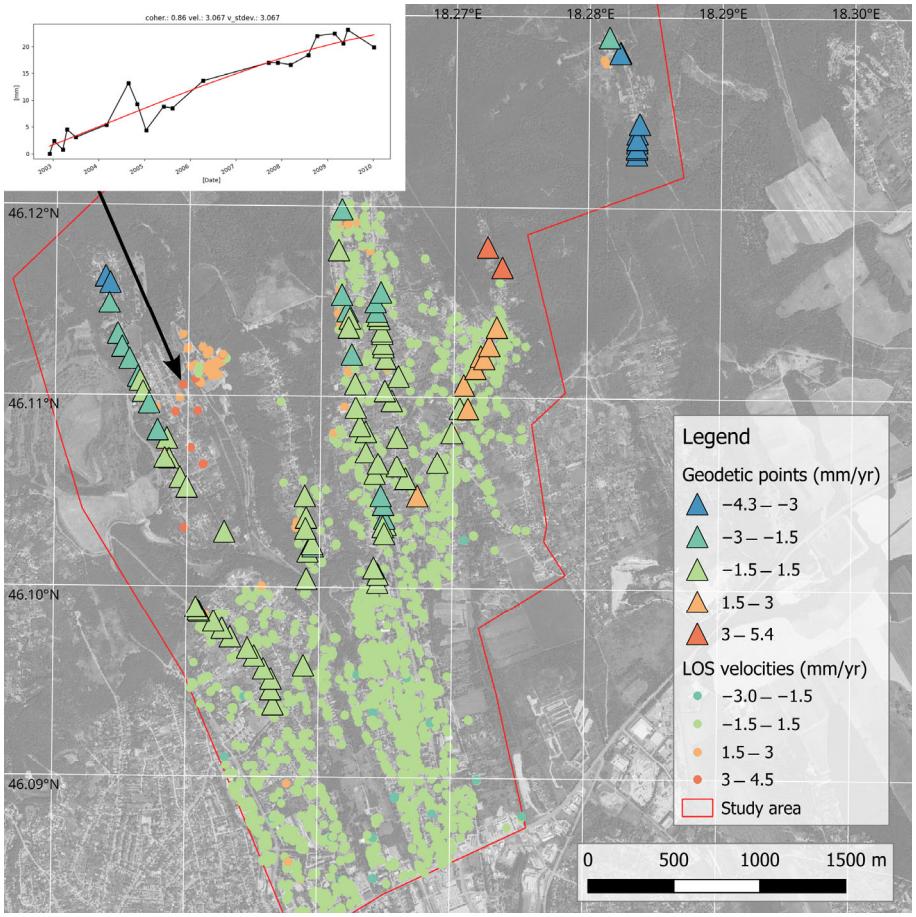


Figure 10. The annual velocity of the PS points compared with the measured average annual displacements of the geodetic points from 2001 until 2010, covering the Envisat acquisitions. The inset graph (top left) displays the displacement time series for a selected PS point indicated by the black arrow, where the red line represents the fitted linear velocity trend.

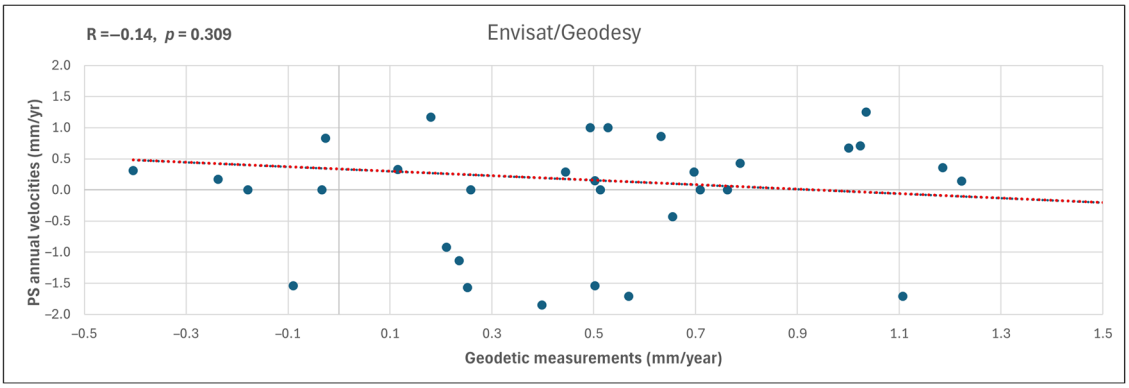


Figure 11. A scatter plot of the geodetic points from the Envisat period and the PS points averaged within their 30 m buffer zones. The red dashed line indicates the linear trendline.

Beyond general fluctuations, several distinct spatial patterns emerged. In Pécsbánya (western area), the geodetic measurements indicated ~2 mm/year of subsidence, while data from scatterers located just 300 m away showed 2–4 mm/year of uplift, likely reflecting residual effects of the extensive uplift observed here in the 1990s. In Mecsekszabolcs (eastern area), geodetic records captured a minor uplift of ~2 mm/year, which was not reflected in the PS velocities despite the high point density. Conversely, in István-akna

(northeast), the geodetic data documented a consistent 3 mm/year subsidence, which was also not corroborated by the InSAR results, due to insufficient PS point coverage.

Continuous hydrogeological records bridge the 2010–2014 observational gap between the Envisat and Sentinel-1 missions. Monitoring wells indicate the water table of the MCFA reached pre-mining equilibrium shortly after 2010. The alignment of these independent datasets confirms that the primary phase of post-mining surface movement concluded during this interval.

For the Sentinel-1 era from 2014, 706 PS points fell within 30 m of 116 geodetic points with sufficient temporal overlap (Figure 12).

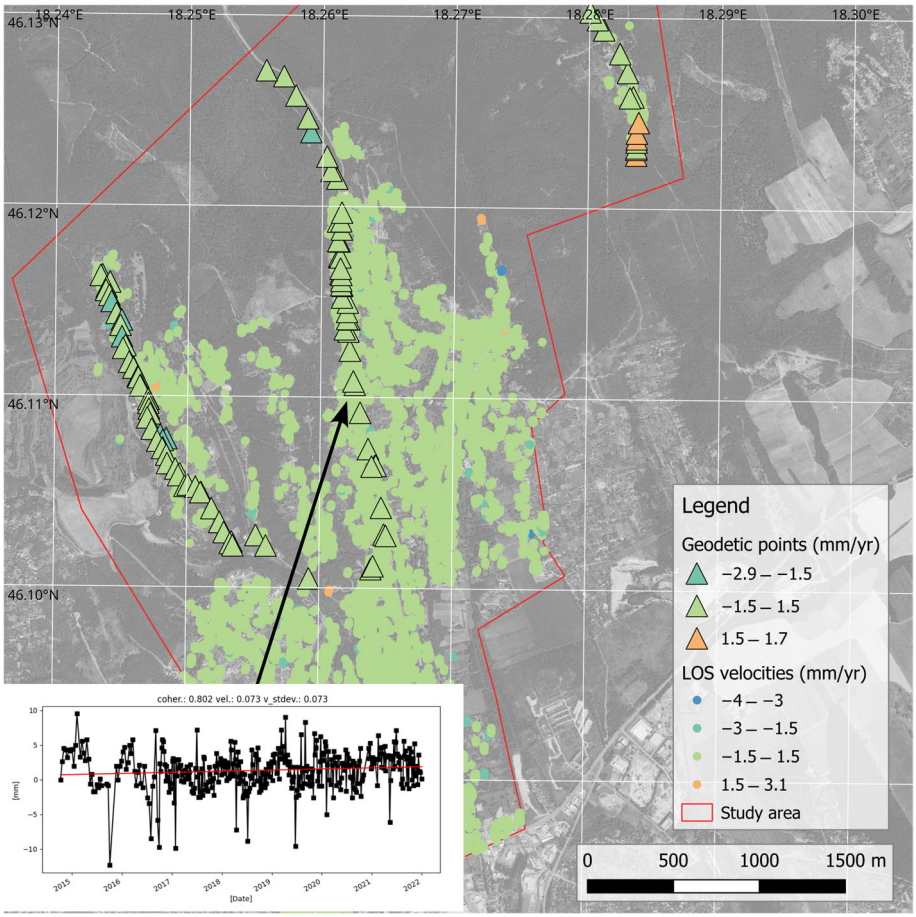


Figure 12. The annual velocity of the PS points compared with the measured average annual displacements of the geodetic points from 2014 until 2022, covering the Sentinel-1 acquisitions. The inset graph (bottom left) displays the displacement time series for a selected PS point indicated by the black arrow, where the red line represents the fitted linear velocity trend.

The comparative analysis demonstrates a marked increase in statistical congruence. The correlation coefficient reached $p = 0.65$ with high statistical significance ($p < 0.001$), while the absolute RMSE was 0.781 mm (Figure 13). Within a geodetic range of 4.47 mm, the resulting normalised RMSE was 17.46%. The distribution of calculated discrepancies confirms that the vast majority of residual movements remain within the sub-millimetric range, reflecting a drastic improvement over earlier measurements.

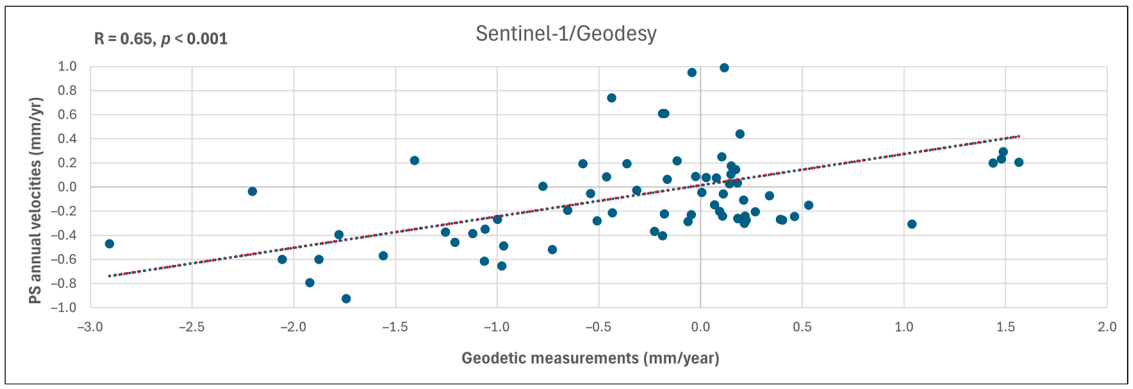


Figure 13. A scatter plot of the geodetic points from the Sentinel period and the PS points averaged within their 30 m buffer zones. The red dashed line indicates the linear trendline.

Regression Kriging

RK was calculated for all three comparisons, resulting in three distinctly different implementation of the surface conditions. The application on the legacy ERS and Envisat datasets (1992–2010) proved inconclusive due to the lack of statistically significant linear relationship between the primary and the auxiliary variables (R = 0.28 and −0.14). Furthermore, the sparse spatial configuration of the geodetic measurement lines relative to the extent of the study area also hindered the process, with inter-line distances frequently exceeding 500 m, thus less than ideally representative of the study area from a statistical point of view [56]. This spatial sparsity specifically resulted in the development of highly extrapolated artefacts, which were exacerbated by the non-uniform point distribution and low precision of the 1990s geodetic network, where measurement noise and theoretical errors often obscured or even exceeded the actual deformation trends [39].

Despite these limitations, the applied geostatistical approach provided a deeper statistical analysis of the relationship between InSAR-derived velocities and geodetic levelling, reinforcing the clear evolutionary shift in data quality and spatial reliability across the three satellite generations (Table 3).

Table 3. The descriptive statistics of Regression Kriging are given for each era. The sample size is the points of the geodetic network, with temporally comparable measurements to their respective PS-InSAR pairs.

Sensor/Era	Samples (*n*)	R^2	Adj. R^2	Std. Error	F-Value	*p*
ERS (1990s)	112	0.055	0.046	1.356	6.41	<0.05
Envisat (2000s)	99	0.250	0.234	1.575	16.02	<0.001
Sentinel-1 (from 2014)	116	0.193	0.186	0.885	27.38	<0.001

The ERS-era processing yielded the weakest results, with minimal agreement and a negligible determination coefficient (R^2 = 0.055). Despite this, the results are technically significant ($p < 0.05$), although the low F-value (6.41) and high standard error indicate that the Kriging interpolation was statistically inadequate to provide a reliable prediction for the surface deformations, thus mathematically proving that the ERS-era Kriging was unstable.

Regarding the Envisat-era (2002–2010), the only measurable improvement was evident in the increase in the R^2 (0.25), which is a realistic value considering the input data, which shows a clear but noisy relationship, underlined by the highest standard error (1.56) of all three calculations. The high residual variance indicates that, while the overall deformation intensity declined, the individual measurements remained noisy.

The Sentinel-1 era (after 2014) represents the most reliable phase of the study, delivering optimal stability and precision for geostatistical integration. Although the R^2 (0.193) is slightly lower than that of the Envisat period, with a drastic reduction in standard error to 0.88 mm, it underscores a significant improvement in measurement consistency, especially considering the high statistical significance ($p < 0.001$) and the robust initial correlation (R = 0.65), demonstrating that the study area reached a critical threshold to stability. Moreover, the RK-derived surface raster fell almost entirely within the uniform velocity threshold of ± 1.5 mm/year employed in this research. These figures highlight a clear technological advancement, especially considering the fact that the geodetic network has become even more sparse after its redesign in 2008, proving that the data quality successfully compensated for the reduced spatial sampling.

The transition from ERS to Sentinel-1 highlights a distinct technological shift towards a precise low-error alignment. These findings are consistent with research indicating that legacy SAR missions often lacked the temporal resolution and coherence for robust geostatistical fusion, particularly when integrated with sparse geodetic networks [57]. Ultimately, the inter-line distance of the low-order legacy levelling network also hindered reliable variogram estimation and triggered extrapolation artefacts, leading to an unfortunate statistical decoupling where the otherwise spatially superior InSAR predictors were unable to improve the spatial interpolation of the levelling data [56].

3.3. Monitoring Wells

The regeneration of the MCFA was a non-uniform spatiotemporal process, with initial recovery rates of 35–50 cm/day in the 1990s decelerating to approximately 10 cm/day before starting to reach stabilisation in the late 2000s [40]. While the regional hydrogeological model suggests that the recharge initiated in the south at lower elevations and attenuated northward following the topography, the process exhibited significant local spatial variability [37]. This heterogeneity reflects the complex response of the multi-layered confined aquifer system and localised hydrogeological conditions. Nevertheless, this timeline closely aligns with observed ERS and Envisat PS-InSAR velocity trends, confirming the return of most monitoring wells to pre-mining equilibrium by 2010 [38,40], as later exhibited by the Sentinel-1 data processing.

In contrast, the groundwater levels transitioned into a stable state prior to the artesian water table, thus characterised only by minor seasonal fluctuations in the processed datasets after 2006. Correlation analysis of the groundwater levels at monitoring wells with nearby Sentinel-1 PS point velocities yielded generally weak-to-moderate positive linear relationships between InSAR-derived deformation and groundwater levels (R = 0.08–0.43), with both data exhibiting minor detrended fluctuations during an overall stable period. The application of a 30-day temporal lag modestly improved these values by a maximum of 0.10, indicating a minor delayed hydrogeological response in specific locations. Figure 14 highlights the strongest observed correspondence at monitoring well 'GW10'.

On the other hand, the MCFA and its potentiometric surface remained statistically decoupled from PS point velocities ($R < 0.1$, $p > 0.05$). Since both the artesian water levels and the surface deformations reached a state of equilibrium by 2010s, the residual fluctuations are minor and are without a common driving trend. This independence is associated with the regional stratigraphy: the impermeable Badenian layers—for most of the study area—create a hydraulic and geomechanical buffer that prevents the transmission of any minor potentiometric oscillations of the aquifer as measurable ground deformation.

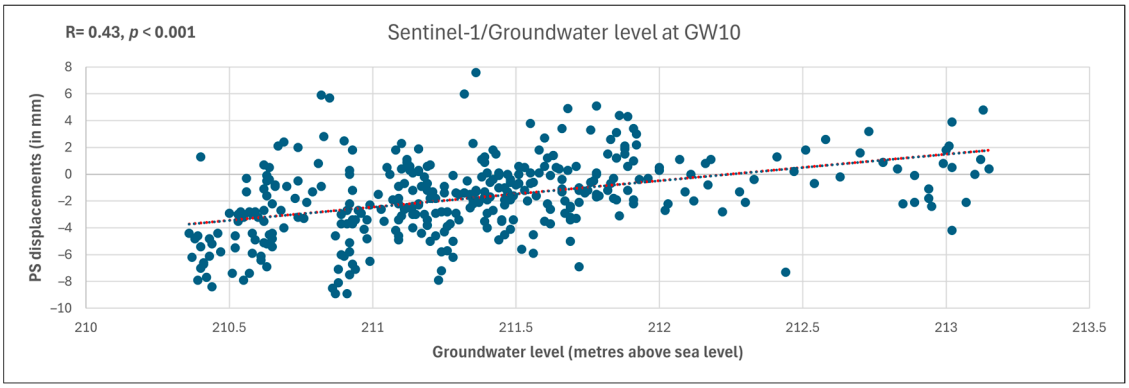


Figure 14. A scatter plot of inter-acquisition displacement velocities of Sentinel-1 PS points surrounding the GW10 monitoring well. The red dashed line indicates the linear trendline.

This interpretation of regional stability is reinforced by the distribution of residential damage reports, which also remained unrelated to any measured hydrological changes (Figure 15). The sole exception was a localised spike in water-related claims during an extreme precipitation event in spring 2010. Notably, these claims originated from a single street situated well outside any identified deformation zones, confirming they were driven by site-specific drainage issues rather than deep-seated geodynamic or hydrogeological processes.

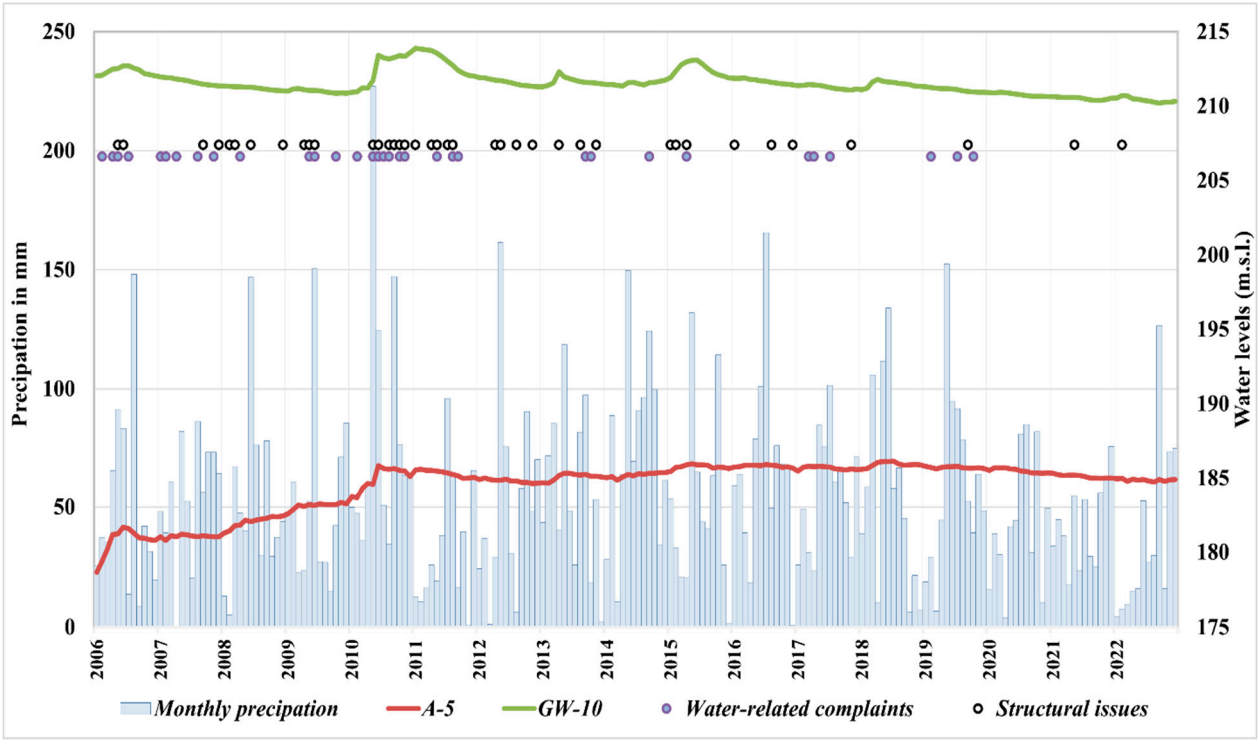


Figure 15. The temporal variation in water levels in a groundwater well (GW-10) and an artesian monitoring well (A-5) in relation to total monthly precipitation between 2006 and 2022. The locations of the wells are shown in Figure 5. Overlaid dots represent filed complaints, color-coded by type (water-related damage in purple, structural problems in black) and plotted chronologically across the same period.

Following a multi-factor framework for identifying drivers of spatiotemporal heterogeneity [58], the stabilisation is attributed to a fundamental shift in the underlying physical

mechanisms. In the study area, the process transitioned from a primary phase of uplift—driven by 1990s aquifer restoration—followed by a secondary phase of slight geomechanical adjustments beginning in the 2000s before the apparent stabilisation. Consequently, the 3 mm/year subsidence at István-akna during the 2010s is in connection with a localised hydrogeological process rather than broader regional trends. This is supported by data from artesian monitoring well A-9 of István-akna, which recorded a mild potentiometric decline in the late 2010s as part of a broader fluctuations over the measured timeline.

3.4. Building Damages

The case file evaluations from the BVH inventory confirmed that approximately two-thirds of the claims over the past three decades were linked to groundwater-related issues, consistent with earlier technical evaluations [38]. Another key contributing factor—either independently or in combination with water damage, was the presence of a swelling clay layer at foundation depth, requiring deep or reinforced foundations and adequate drainage to mitigate seasonally induced vertical movements. Structural damage was most severe in older single-storey buildings with partial basements, where the differential rigidity between the basement and ground floor segments often induced structural stress and caused failure [39].

During the ERS period, 478 complaints were filed, peaking at 119 in 2001. An additional 236 claims were registered during the Envisat era, while only 15 new cases were reported after 2010. The annual distribution and resolution of all complaints analysed are shown in Figure 16.

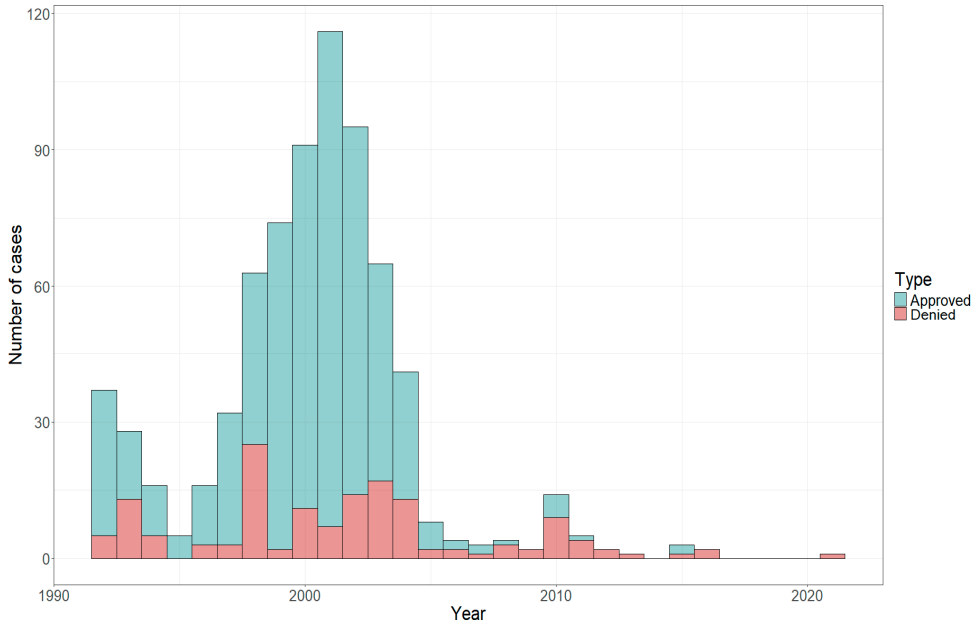


Figure 16. The temporal distribution of the filed complaints coloured according to their final status.

Deformation Zones

To evaluate spatial patterns of damage attribution, deformation zones were delineated by interpolating velocity values from both InSAR and geodetic datasets. These zones showed only partial spatial overlap in the 1990s and 2000s, reflecting methodological differences in how surface displacements were captured.

In the 1990s, damage claims located within the ERS-based InSAR deformation zone had a notably high acceptance rate of over 90% (399 accepted vs. 43 denied), while claims outside this zone were accepted in only 25.5% of cases. In contrast, the geodetic-based zone produced a less distinctive pattern: although 91.7% of claims within the zone

were accepted, the acceptance rate outside it remained relatively high at 81.1%, despite substantial differences in the zones' spatial extent (Figure 17).

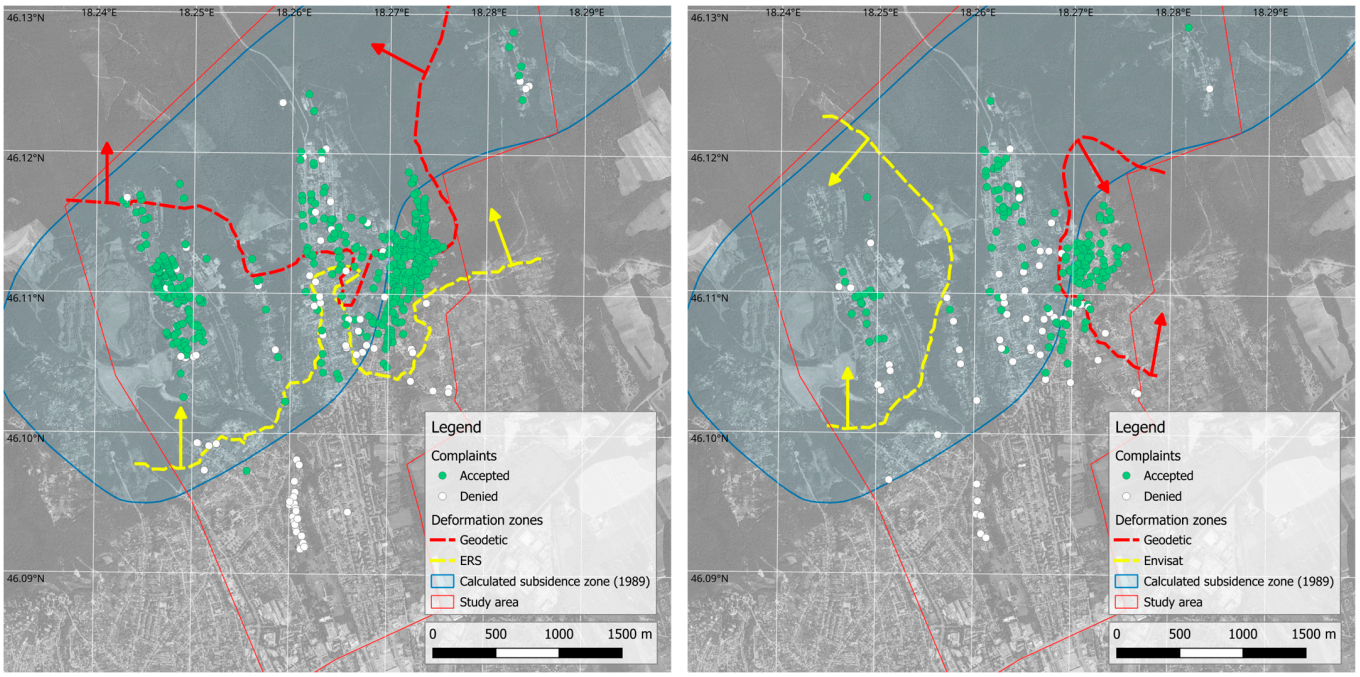


Figure 17. Distribution of damage according to the designated zones, based on interpolated movements derived from geodetic measurements and the ERS (**left**) and Envisat (**right**) data. The dashed lines with arrows indicate the boundaries and extent of the deformation zones.

In the 2000s, deformation zones delineated from InSAR and geodetic data showed no spatial overlap, with the InSAR-based zone concentrated in the west and the geodetic zone in the east. The InSAR zone yielded a moderate claim acceptance rate of 75.9%, nearly identical to the 73.1% observed outside it. In contrast, the geodetic zone exhibited a markedly higher acceptance rate of 93.6%, compared with 59.9% outside (n = 236). Notably, claims submitted from within the officially designated 1989 subsidence zone were accepted at a significantly lower rate than those from outside (Table 4).

Table 4. The results of the decisions in each case, as a percentage of the total number of cases, and according to their respective locations: inside or outside of each defined deformation zone. (ERS-era: n = 478; Envisat-era: n = 236).

Location	Outcome	ERS Era (1992–2001)			Envisat Era (2002–2010)		
		InSAR	Geodesy	Subsidence Zone	InSAR	Geodesy	Subsidence Zone
Inside the zone	accepted	90.9%	91.7%	85.4%	75.9%	93.6%	64.8%
	denied	9.1%	8.3%	14.6%	24.1%	6.4%	35.2%
Outside the zone	accepted	25.5%	81.1%	83.6%	73.1%	59.9%	82.6%
	denied	74.5%	18.9%	16.4%	26.9%	40.1%	17.4%

In the three-year gap between the Envisat and Sentinel operational periods, only nine new complaints were recorded, all from the central or western parts of the study area; eight concerned structural damage, but only one was partially compensated. During the Sentinel period (2014–2022), the PS-InSAR data indicated unprecedented overall stability, with over 95% of the PS velocities ranging between −1 and +1 mm/year. Concurrent

geodetic measurements confirmed this trend, with deviations not exceeding ±3 mm/year. Six additional claims—primarily for structural damage—emerged from the Pécsbánya district, which previously showed notable PS point velocities (3.5 mm/year) during the Envisat era but was stable when these latest complaints arose.

4. Discussion

In this study, the spatiotemporal evolution of post-mining surface deformation was characterised through a comparative assessment. While the broad comparison provided essential context, the main aim was to identify the spatial patterns and temporal evolution of ground displacements associated with the mine closure and prove the eventual cessation of post-mining uplift. To support this analysis, additional datasets were analysed, including relevant information from comprehensive hydrogeological modelling, monitoring well datasets, and an in-depth review of residential complaints concerning water and structural damage to properties. Alongside extensive cross-comparisons, Regression Kriging was also implemented, attempting to integrate the heterogeneous geodetic and InSAR datasets.

4.1. The ERS-Era (1992–2001)

During the early years of the hydrostatic rebound, the InSAR datasets provided a robust and spatially consistent characterisation of surface velocity patterns, enabling a detailed assessment of deformation across the study area. In contrast, the levelling network operating in the 1990s exhibited substantial variability and fluctuations, often exceeding the InSAR-measured annual velocities, indicating that these low-order geodetic configurations were highly susceptible to environmental factors, often obscuring the underlying signal of post-mining deformation. A major source of variability in the geodetic measurements was caused by the volumetric changes in the subsoil according to fluctuations of seasonal moisture, which in fact had not been accounted for during the network's initial design [39]. These soil dynamics introduced vertical displacements unrelated to mining activity, complicating the interpretation of levelling data. Even following the 2008 network renewal—which transitioned the framework to high-order levelling—some residual anomalies persisted. These were likely influenced by inadequate foundation conditions at benchmark locations, many of which were not designed with local geotechnical properties in mind. These findings underscore a key limitation of legacy levelling surveys in such environments: despite their theoretical precision, their reliability may be compromised by near-surface geological variability.

4.2. The Envisat Era (2002–2010)

The apparent lack of correlation in the Envisat era ($R = -0.14$) serves as a statistical confirmation of the progressive surface stabilisation rather than a methodological failure. As the high-velocity hydrostatic rebound of the 1990s began to dissipate—characterised by gradual consolidation, a year-on-year reduction in uplift rates, and a progressive spatial contraction of the affected zones—the weakening deformation was effectively overwhelmed by the precision limits of the legacy geodetic network.

Despite this apparent noise, notable localised differences also persisted, most prominently near the former István-akna mining shaft. In this peripheral zone, levelling detected measurable subsidence during the Envisat era, whereas PS-InSAR failed to capture corresponding deformations. This inconsistency highlights one core limitation of PS-InSAR: the critical reduction in PS point density in vegetated sporadically built environments, such as István-akna. Consequently, in such abandoned or overgrown peripheral areas, traditional geodetic levelling remains essential to provide data where the small number of

stable scatterers prevents the calculation of reliable PS-InSAR data, thus allowing for the uncovering of the movement history for the vicinity.

4.3. The Sentinel-1 Era

The results from the Sentinel-1 era represent a significant advancement in consistency compared to previous observations. The improvement is quantified by the attainment of sub-millimetric residuals (RMSE = 0.78 mm), marking the successful alignment of satellite and geodetic monitoring systems. Statistical analysis indicates that the transition to a post-2008 high-order levelling network yielded highly congruent results, exhibiting a statistically significant correlation with the Sentinel-1-based measurements across the study area. Furthermore, the apparent stability of PS annual velocities perfectly mirrors the cessation of regional movements. Ultimately, these results demonstrate that PS-InSAR, when supported by a renewed geodetic framework that accounts for load-bearing stability, is a high-fidelity tool capable of monitoring the most subtle phases of geomechanical stabilisation.

The progressive shift from surface deformation to stability in Regression Kriging performance between the legacy and modern eras highlights a fundamental shift in the reliability of multi-sensor data fusion for post-mining monitoring. While the legacy ERS and Envisat datasets exhibited high stochastic variability and low information density—rendering stable variogram estimation mathematically non-viable, the Sentinel-1-era calculations achieved a critical threshold of measurement precision and a submillimetric standard error. This confirms that the observed stabilisation of the Pécs mining district is not a mathematical artifact of the interpolation but a physically grounded reality, where the geostatistical model and the hydrogeological recovery have successfully converged

4.4. Monitoring Wells and Residential Claims

Both measurement techniques, albeit capturing different aspects, consistently revealed a steady decline in displacement velocities across the study area, indicating the gradual cessation of mining-induced ground movements. This trend is independently confirmed by monitoring well datasets and hydrogeological modelling [37]. Water levels in the artesian aquifer largely recovered to their presumed pre-mining levels by the early 2010s, with recharge initiating in lower elevations before attenuating northward according to the topography. This pattern closely aligns with the progressive contraction of deformation zones observed in the InSAR time series and the geodetic measurements. The spatial and temporal concordance among these independent datasets confirms that uplift was primarily driven by the hydrostatic rebound, following the cessation of dewatering. The statistical analysis reinforces this conclusion, showing that post-2010 measurements exhibit no discernible deformation trends, only minor fluctuations, providing weak correlations with groundwater fluctuations (R = 0.08–0.43) and no significant relationship with artesian water levels. This indicates that surface conditions have reached a state of stability.

Notably, comparisons with building damage and water-related residential complaints reveal that the submitted claims do not spatially correlate with the interpolated deformation zones. Furthermore, temporal peaks in water damage claims do not align with aquifer recharge or surface deformations, suggesting that these were not primary causes of building damage. This explains the small number (<10) of claims observed after regional stabilisation; these cases are primarily tied to the specific vulnerability of older (usually pre-1950s constructions) single-storey buildings with shallow or partial basements. The differential rigidity of these constructions makes them highly sensitive to the volumetric changes of near-surface swelling clay layers, which appear to be the main contributors to the observed damage rather than broader deep-seated geodynamic processes. The damage reported—

primarily diagonal cracking in load-bearing walls—matches the classic signature of the volumetric changes in the swelling clay layer identified in technical reports. Ultimately, the overall reduction in claims has been driven by improved local water management—including enhanced drainage and targeted groundwater pumping—and the adoption of modern construction practices with robust foundations.

4.5. Discussion Summary

Our results indicate that high-order levelling provides the consistency and high-fidelity precision necessary to serve as a robust cross-validation tool for InSAR under the specific conditions of the study area. By leveraging the strengths and compensating for the limitations of both InSAR and geodetic techniques, a more comprehensive understanding of post-mining deformation was achieved. Notably, the findings demonstrate that geomechanical stability has been established throughout the study area since 2010s. The absence of displacements in the most recent datasets—which exhibit only minor non-directional fluctuations—confirms that the uplift triggered by the cessations of long-term dewatering and the subsequent recovery of artesian water levels have fully ceased.

The combined use of geodetic and InSAR techniques provides complementary insights that offer reliable basis for risk mitigation, and the objective evaluation of damage claims. The methodology presented here may be readily applied to other mining-affected urban areas, offering a transferable framework for long-term deformation assessment and supporting more informed data-driven land-use planning and resilience strategies.

5. Conclusions

Our research has demonstrated that integrating InSAR data into complex deformation monitoring scenarios offers substantial advantages, providing a level of spatial detail and coverage that fixed point geodetic networks alone cannot achieve. This enhanced spatial resolution not only improves the delineation and understanding of mining-induced surface deformation phenomena but also highlights the inherent limitations of traditional low-order monitoring networks, which often lack the precision necessary to resolve subtle non-linear movements.

Beyond its scientific contributions, and the technical validation, such integrated monitoring approaches deliver practical value to local authorities by supplying reliable objective input for a data-driven decision-making process about land-use planning and infrastructure development. These insights are equally vital at a residential level for the fair and transparent evaluation of damage claims related to mining-induced ground deformations, ultimately enabling more effective resource allocation and remediation strategies.

In conclusion, the comprehensive monitoring of current and former mining areas is best achieved through multi-sensor data fusion strategies. Our findings emphasise that while lower-order geodetic data may provide insufficient resolution for high-fidelity cross-validation, the combination of PS-InSAR with high-order geodetic techniques yields highly congruent results. Leveraging these complementary capabilities represents a significant advancement in the monitoring of subsidence and surface deformation, facilitating more informed decision-making and supporting the sustainable management of mining-impacted regions, particularly considering recent transformations within Europe's energy landscape.

Author Contributions: Conceptualisation: I.P.K. and D.M.K.; methodology: I.P.K. and D.M.K.; software: L.R. and I.P.K.; validation: I.P.K. and D.M.K.; formal analysis: I.P.K. and D.M.K.; investigation: D.M.K.; resources: L.R., D.M.K. and I.P.K.; data curation: D.M.K. and I.P.K.; writing—original draft preparation: D.M.K.; writing—review and editing: D.M.K. and I.P.K.; visualisation: D.M.K.; supervision: I.P.K.; project administration: D.M.K.; funding acquisition: D.M.K. All authors have read and agreed to the published version of the manuscript.

Funding: This research received no external funding.

Data Availability Statement: The original contributions presented in this study are included in the article. Further inquiries can be directed to the corresponding author.

Acknowledgments: The authors are grateful to Sándor Pali of the BVH, who provided data, scientific support, and thorough advice about the research.

Conflicts of Interest: The authors declare no conflicts of interest. Authors Dr. István Péter Kovács and Dr. Levente Ronczyk are employed by the DATelite Ltd. The remaining author declare that the research was conducted in the absence of any commercial or financial relationships that could be construed as a potential conflict of interest. The DATelite Ltd. had no role in the design of the study; in the collection, analyses, or interpretation of data; in the writing of the manuscript, or in the decision to publish the results.

References

1. Yan, W.; Guo, J.; Yan, S. Difference in Surface Damage between Deep and Shallow Mining of Underground Coal Resources in China. *Sustainability* **2023**, *15*, 7296. [CrossRef]
2. Ma, Z.; Yang, X.; Xie, L.; Dong, W. Life Cycle Mining Deformation Monitoring and Analysis Using Sentinel-1 and Radarsat-2 InSAR Time Series. *Remote Sens.* **2024**, *16*, 2335. [CrossRef]
3. Agboola, O.; Babatunde, D.E.; Fayomi, O.S.I.; Sadiku, E.R.; Popoola, P.; Moropeng, L.; Yahaya, A.; Mamudu, O.A. A review on the impact of mining operation: Monitoring, assessment and management. *Results Eng.* **2020**, *8*, 100181. [CrossRef]
4. Barra, A.; Reyes-Carmona, C.; Herrera, G.; Galve, J.P.; Solari, L.; Mateos, R.M.; Azañón, J.M.; Béjar-Pizarro, M.; López-Vinielles, J.; Palamà, R.; et al. From satellite interferometry displacements to potential damage maps: A tool for risk reduction and urban planning. *Remote Sens. Environ.* **2022**, *282*, 113294. [CrossRef]
5. Maj, A. Rock-Mass Movement Monitoring System in Historical Salt Mines, Using the Example of the Bochnia Salt Mine. *Procedia Eng.* **2017**, *191*, 496–503. [CrossRef]
6. Walerysiak, N.; Blachowski, J.; Kujawa, P.; Wajs, J.W. Monitoring and Analysis of Ground Movements in the Babina Post-Mining Area. *Civ. Environ. Eng. Rep.* **2025**, *35*, 258–279. [CrossRef]
7. Mancini, F.; Stecchi, F.; Gabbianelli, G. GIS-based assessment of risk due to salt mining activities at Tuzla (Bosnia and Herzegovina). *Eng. Geol.* **2009**, *109*, 170–182. [CrossRef]
8. Hui, X.; Ma, F.; Zhao, H.; Xu, J. Monitoring and statistical analysis of mine subsidence at three metal mines in China. *Bull. Eng. Geol. Env.* **2019**, *78*, 3983–4001. [CrossRef]
9. Rodriguez-Lloveras, X.; Puig-Polo, C.; Lantada, N.; Gili, J.A.; Marturia, J. Two decades of GPS/GNSS and DInSAR monitoring of Cardona salt mines (NE of Spain)—Natural and mining-induced mechanisms and processes. *Proc. Int. Assoc. Hydrol. Sci.* **2020**, *382*, 167–172. [CrossRef]
10. Xue, C.; Psimoulis, P.; Zhang, Q.; Meng, X. Analysis of the performance of closely spaced low-cost multi-GNSS receivers. *Appl. Geomat.* **2021**, *13*, 415–435. [CrossRef]
11. Fan, W.; Pan, G.; Wang, L. Development and Application of a Networked Automatic Deformation Monitoring System. *J. Geovisualization Spat. Anal.* **2020**, *4*, 11. [CrossRef]
12. Yang, X.; Zhou, Z.; Yang, Y.; Yao, X.; Liu, C.; Liu, L.; Xie, S. GNSS-Based Monitoring Methods for Mining Headframes. *Appl. Sci.* **2025**, *15*, 4368. [CrossRef]
13. Ferretti, A.; Prati, C.; Rocca, F. Permanent scatterers in SAR interferometry. *Trans. Geosci. Remote Sens.* **2001**, *39*, 8–20. [CrossRef]
14. Crosetto, M.; Monserrat, O.; Iglesias, R.; Crippa, B. Persistent scatterer interferometry: Potential, limits, and initial C- and X-band comparison. *Photogramm. Eng. Remote Sens.* **2010**, *76*, 1061–1069. [CrossRef]
15. Giorgini, E.; Orellana, F.; Arratia, C.; Tavasci, L.; Montalva, G.; Moreno, M.; Gandolfi, S. InSAR Monitoring Using Persistent Scatterer Interferometry (PSI) and Small Baseline Subset (SBAS) Techniques for Ground Deformation Measurement in Metropolitan Area of Concepción. *Chile. Remote Sens.* **2023**, *15*, 5700. [CrossRef]
16. Cigna, F.; Esquivel Ramírez, R.; Tapete, D. Accuracy of Sentinel-1 PSI and SBAS InSAR Displacement Velocities against GNSS and Geodetic Levelling Monitoring Data. *Remote Sens.* **2021**, *13*, 4800. [CrossRef]
17. Pasquali, P.; Cantone, A.; Riccardi, P.; Defilippi, M.; Ogushi, F.; Gagliano, S.; Tamura, M. Mapping of ground deformations with interferometric stacking techniques. In *Land Applications of Radar Remote Sensing*; Holecz, F., Pasquali, P., Milisavljevic, N., Eds.; InTechOpen: London, UK, 2014; pp. 231–258.
18. Cigna, F.; Bianchini, S.; Casagli, N. How to assess landslide activity and intensity with Persistent Scatterer Interferometry (PSI): The PSI-based matrix approach. *Landslides* **2013**, *10*, 267–283. [CrossRef]

19. Kovács, I.P.; Bugya, T.; Czigány, S.; Defilippi, M.; Lóczy, D.; Riccardi, P.; Ronczyk, L.; Pasquali, P. How to avoid false interpretations of Sentinel-1A TOPSAR interferometric data in landslide mapping? A case study: Recent landslides in Transdanubia, Hungary. *Nat. Hazards* **2018**, *96*, 693–712. [CrossRef]
20. Pepe, S.; D'Auria, L.; Castaldo, R.; Casu, F.; De Luca, C.; De Novellis, V.; Sansosti, E.; Solaro, G.; Tizzani, P. The Use of Massive Deformation Datasets for the Analysis of Spatial and Temporal Evolution of Mauna Loa Volcano (Hawai'i). *Remote Sens.* **2018**, *10*, 968. [CrossRef]
21. Raspini, F.; Bianchini, S.; Ciampalini, A.; Del Soldato, M.; Solari, L.; Novali, F.; Del Conte, S.; Rucci, A.; Ferretti, A.; Casagli, N. Continuous, semi-automatic monitoring of ground deformation using Sentinel-1 satellites. *Sci. Rep.* **2018**, *8*, 7253. [CrossRef]
22. Nappo, N.; Peduto, D.; Polcari, M.; Livio, F.; Ferrario, M.F.; Comerci, V.; Stramondo, S.; Michetti, A.M. Subsidence in Como historic centre (northern Italy): Assessment of building vulnerability combining hydrogeological and stratigraphic features, Cosmo-SkyMed InSAR and damage data. *Int. J. Disaster Risk Reduct.* **2021**, *56*, 102115. [CrossRef]
23. Semenzato, A.; Pappalardo, S.E.; Codato, D.; Trivelloni, U.; De Zorzi, S.; Ferrari, S.; De Marchi, M.; Massironi, M. Mapping and Monitoring Urban Environment through Sentinel-1 SAR Data: A Case Study in the Veneto Region (Italy). *ISPRS Int. J. Geo-Inf.* **2020**, *9*, 375. [CrossRef]
24. Heleno, S.I.N.; Oliveira, L.G.S.; Henriques, M.J.; Falcão, A.P.; Lima, J.N.P.; Cooksley, G.; Ferretti, A.; Fonseca, A.M.; Lobo-Ferreira, J.P.; Fonseca, J.F.B.D. Persistent scatterers interferometry detects and measures ground subsidence in Lisbon. *Remote Sens. Environ.* **2011**, *115*, 2152–2167. [CrossRef]
25. Dobos, E.; Kovács, I.P.; Kovács, D.M.; Ronczyk, L.; Szűcs, P.; Perger, L.; Mikita, V. Surface Deformation Monitoring and Risk Mapping in the Surroundings of the Solotvyno Salt Mine (Ukraine) between 1992 and 2021. *Sustainability* **2022**, *14*, 7531. [CrossRef]
26. Caro Cuenca, M.; Hooper, A.J.; Hanssen, R.F. Surface Deformation Induced by Water Influx in the Abandoned Coal Mines in Limburg, The Netherlands Observed by Satellite Radar Interferometry. *J. Appl. Geophys.* **2013**, *88*, 1–11. [CrossRef]
27. Blachowski, J.; Kopeć, A.; Milczarek, W.; Owczarz, K. Evolution of secondary deformations captured by satellite radar interferometry: Case study of an abandoned coal basin in SW Poland. *Sustainability* **2019**, *11*, 884. [CrossRef]
28. Declercq, P.-Y.; Dusar, M.; Pirard, E.; Verbeurgt, J.; Choopani, A.; Devleeschouwer, X. Post Mining Ground Deformations Transition Related to Coal Mines Closure in the Campine Coal Basin, Belgium, Evidenced by Three Decades of MT-InSAR Data. *Remote Sens.* **2023**, *15*, 725. [CrossRef]
29. Colesanti, C.; Mouelic, S.L.; Bennani, M.; Raucoules, D.; Carnec, C.; Ferretti, A. Detection of mining related ground instabilities using the Permanent Scatterers technique—A case study in the east of France. *Int. J. Remote Sens.* **2005**, *26*, 201–207. [CrossRef]
30. Malinowska, A.A.; Witkowski, W.T.; Guzy, A.; Hejmanowski, R. Satellite-Based Monitoring and Modeling of Ground Movements Caused by Water Rebound. *Remote Sens.* **2020**, *12*, 1786. [CrossRef]
31. Tzampoglou, P.; Loukidis, D.; Koulermou, N. Seasonal Ground Movement Due to Swelling/Shrinkage of Nicosia Marl. *Remote Sens.* **2022**, *14*, 1440. [CrossRef]
32. Rey-Martí, A.; Valencia-Toledo, A.; Chaparro-Banegas, N.; Mas-Tur, A.; Roig-Tierno, N. Developing models to assess the social impact of mining: An exploratory study trough necessary conditions analysis (NCA). *Resour. Pol.* **2023**, *83*, 103704. [CrossRef]
33. Florkowska, L.; Bryt-Nitarska, I. Social Responsibility of Science in the Sustainable Development of Mining and Post-Mining Areas. *Appl. Sci.* **2026**, *16*, 776. [CrossRef]
34. Lovász, G.; Nagyváradi, L. The function of the natural resources in the development of Pécs and Komló [A természeti erőforrások változó szerepe Pécs és Komló fejlődésében]. In *Papers from the Department of Physical Geography, Institute of Geography [Közlemények A PTE Természetföldrajzi Tanszékéről]*; University of Pécs: Pécs, Hungary, 2000; Volume 13, pp. 1–11.
35. Lóczy, D.; Nagyváradi, L.; Gyenizse, P.; Pirkhoffer, E.; Dezső, J. Umweltfolgen und Rekultivierung in Steinkohlenbergbaugebieten. In *Arbeitsmaterialien zur Raumordnung und Raumplanung Heft 243*; Aubert, A., Tóth, J., Eds.; Universität Bayreuth: Bayreuth, Germany, 2006; pp. 65–78.
36. Erdősi, F. Antropogén módosulások a természeti környezetben. In *Baranya Megye Természeti Földrajza*; Lovász, G., Ed.; Baranya Megyei Levéltár: Pécs, Hungary, 1977; 298p.
37. Baranyi, I. *Hidrológiai Helyzetkép és Várható Változások Pécs-Mecsekszabolcs Bányatelken*; Geo-Consult Bt.: Pécs, Hungary, 1998; 25p. (In Hungarian)
38. Juhász, J. *On the Role of the Hydraulic Connectivity of the Abandoned Deep Mines in Pécs-Mecsekszabolcs in the Development of Building Waterlogging [A Felhagyott Pécs-Mecsekszabolcsi Mélyműveléses Bányamezők Hidraulikus Kapcsolatrendszerének Szerepéről, a Pécs-Mecsekszabolcs Településrész Épületvizesedés Bányakárainak Kialakulásában]*; Unpublished manuscript; University of Miskolc: Miskolc, Hungary, 2003; 217p.
39. Somosvári, Z. *Complex Investigation of Surface Movements in the "Pécs-Mecsekszabolcs" Mining Area [Felszínmozgások Komplex Vizsgálata "Pécs-Mecsekszabolcs" Bányatelken]*; Unpublished manuscript; University of Miskolc: Miskolc, Hungary, 2008; 144p.
40. Némedi Varga, Z. (Ed.) *Research and Mining Geology of the Black-Coal Deposit in the Mecsek Mountains [A Mecseki Kőszén Kutatása és Bányaföldtana]*; Central Library and Archives of the University of Miskolc: Miskolc, Hungary, 1995; 471p, ISBN 963-661-262. (In Hungarian)

41. Molnár, L. *Hydraulic Modeling Related to the Infilling of Coal Mining Cavity Systems in the Pécs and Komló Region [Pécs és Komló Térségében a Szénbányászati Üregrendszer Feltöltődésével Kapcsolatos Szivárgáshidraulikai Modellezés—Műszaki Szakértői Tanulmány]*; Smaragd-GSH Ltd.: Budapest, Hungary, 2019; 81p.
42. Hámor, G.; Nagy, E.; Földi, M.A. *Mecsek-Hegység Földtani Térképe. Pécs-Meszes 1:10000*; Magyar Állami Földtani Intézet: Budapest, Hungary, 1965.
43. ESA's Online Dissemination Portal. Available online: https://esar-ds.eo.esa.int/oads/access/collection (accessed on 12 August 2025).
44. Alaska SAR Facility. Available online: https://search.asf.alaska.edu/#/ (accessed on 12 August 2025).
45. Berardino, P.; Fornaro, G.; Lanari, R.; Sansosti, E. A new algorithm for surface deformation monitoring based on small baseline differential SAR interferograms. *IEEE Trans. Geosci. Remote Sens.* **2002**, *40*, 2375–2383.
46. Cerchiello, V.; Tessari, G.; Velterop, E.; Riccardi, P.; Defilippi, M.; Pasquali, P. Building Damage Risk by Modeling Interferometric Time Series. *IEEE Geosci. Remote Sens. Lett.* **2017**, *14*, 509–513. [CrossRef]
47. Macchiarulo, V.; Milillo, P.; Blenkinsopp, C.; Reale, C.; Giardina, G. Multi-temporal InSAR for transport infrastructure monitoring: Recent trends and challenges. *Proc. Inst. Civ. Eng. Bridge Eng.* **2022**, *175*, 92–117. [CrossRef]
48. Blasco, J.M.D.; Foumelis, M.; Stewart, C.; Hooper, A. Measuring urban subsidence in the Rome Metropolitan Area (Italy) with Sentinel-1 SNAP-StaMPS Persistent Scatterer Interferometry. *Remote Sens.* **2019**, *11*, 129. [CrossRef]
49. Ferretti, A.; Fumagalli, A.; Novali, F.; Prati, C.; Rocca, F.; Rucci, A. A new algorithm for processing interferometric data-stacks: SqueeSAR. *IEEE Trans. Geosci. Remote Sens.* **2011**, *49*, 3460–3470. [CrossRef]
50. Fadhillah, M.F.; Achmad, A.R.; Lee, C.-W. Improved Combined Scatterers Interferometry with Optimized Point Scatterers (ICOPS) for Interferometric Synthetic Aperture Radar (InSAR) Time-Series Analysis. *IEEE Trans. Geosci. Remote Sens.* **2022**, *60*, 5220014. [CrossRef]
51. Sowter, A.; Bin Che Amat, M.; Cigna, F.; Marsh, S.; Athab, A.; Alshammari, L. Mexico City land subsidence in 2014–2015 with Sentinel-1 IW TOPS: Results using the intermittent SBAS (ISBAS) technique. *Int. J. Appl. Earth Obs. Geoinf.* **2016**, *52*, 230–242. [CrossRef]
52. Jarvis, A.; Reuter, H.I.; Nelson, A.; Guevara, E. Hole-Filled SRTM for the Globe, Version 4, 2008. Available from the CGIAR-CSI SRTM 90 m Database. Available online: http://srtm.csi.cgiar.org (accessed on 11 March 2026).
53. Hengl, T.; Heuvelink, G.B.; Rossiter, D.G. About regression-kriging: From equations to case studies. *Comput. Geosci.* **2007**, *120*, 75–93. [CrossRef]
54. Lu, C.H.; Ni, C.F.; Chang, C.P.; Yen, J.Y.; Hung, W.C. Combination with precise leveling and PSInSAR observations to quantify pumping-induced land subsidence in central Taiwan. *Proc. Int. Assoc. Hydrol. Sci.* **2015**, *372*, 77–82. [CrossRef]
55. Fuhrmann, T.; Caro Cuenca, M.; Knöpfler, A.; van Leijen, F.J.; Mayer, M.; Westerhaus, M.; Hanssen, R.F.; Heck, B. Estimation of small surface displacements in the Upper Rhine Graben area from a combined analysis of PS-InSAR, levelling and GNSS data. *Geophys. J. Int.* **2015**, *203*, 614–631. [CrossRef]
56. Ibrahim, H.B.; Salah, M.; Zarzoura, F.; El-Mewafi, M. Persistent scatterer interferometry (PSI) technique for road infrastructure monitoring: A case study of the roadway network of the Nile Delta (Egypt). *Innov. Infrastruct. Solut.* **2024**, *9*, 119. [CrossRef]
57. Furst, S.L.; Doucet, S.; Vernant, P.; Champollion, C.; Carme, J.-L. Monitoring surface deformation of deep salt mining in Vauvert (France), combining InSAR and leveling data for multi-source inversion. *Solid Earth* **2021**, *12*, 15–34. [CrossRef]
58. Wang, J.; Hu, J.; Zhou, Z.; Wang, J.; Meng, J.; Pan, D.; Li, P.; Wang, L.; Xiang, J.; Ma, J. Integrating Explainable Machine Learning and LSTM with Multiple Factors for Mechanism Identification and Prediction of Land Deformation in the North Henan Plain. *J. Geovis. Spat. Anal.* **2026**, *10*, 5. [CrossRef]

Disclaimer/Publisher's Note: The statements, opinions and data contained in all publications are solely those of the individual author(s) and contributor(s) and not of MDPI and/or the editor(s). MDPI and/or the editor(s) disclaim responsibility for any injury to people or property resulting from any ideas, methods, instructions or products referred to in the content.